Lithos 382–383 (2021) 105895

Contents lists available at ScienceDirect

Lithos

journal homepage: www.elsevier.com/locate/lithos

Research Article

Petrogenesis of the Main Range and Eastern Province granites in eastern Myanmar: New insights from zircon U–Pb ages and Sr–Nd isotopes

Feng Cong [a,b,*], Fu-Yuan Wu [a], Wen-Chang Li [b], Jian-Gang Wang [a], Fang-Yang Hu [a], De-Feng He [c], Wei-Qiang Ji [a], Wei Lin [a], Kyaing Sein [d]

[a] State Key Laboratory of Lithospheric Evolution, Institute of Geology and Geophysics, Chinese Academy of Sciences, Beijing 100029, China
[b] Chengdu Center of China Geological Survey, Chengdu 610081, China
[c] Institute of Geochemistry, Chinese Academy of Sciences, Guiyang 550002, China
[d] Myanmar Geosciences Society, Yangon, Myanmar

ARTICLE INFO

Article history:
Received 29 August 2020
Received in revised form 15 November 2020
Accepted 18 November 2020
Available online 27 November 2020

Keywords:
Main Range Province
Eastern Province
Zircon U–Pb ages
Sr–Nd isotopes
Eastern Myanmar
Southeast Asia

ABSTRACT

The Main Range and Eastern Provinces are two major granite belts in Southeast Asia. These granite belts extend southward from the southeastern Tibetan Plateau to Myanmar, and through Thailand into Peninsular Malaysia. They are interpreted to represent the magmatic expression of the closure of the Paleo-Tethys from the Permian to the Triassic. Myanmar lies in the heart of these granite belts. The Kyaing Tong and Tachileik granites in the far east of Myanmar are important components of the granite belts of Southeast Asia; however, due to the lack of reliable geochronology within eastern Myanmar, delineation of the Main Range and Eastern Province belts in this region is very poorly constrained. Here we present new zircon U–Pb age, whole-rock composition, and Sr–Nd isotope data from the Kyaing Tong and Tachileik granites from eastern Myanmar to address this geological problem. Measured ages of 207–216 Ma from the Kyaing Tong granites imply that they are a northern extension of the Main Range Province, whereas the Tachileik granites yield ages of 246–250 Ma, which suggests that they are the northern extension of the Eastern Province granite belt. Both belts in eastern Myanmar comprise biotite monzogranites and granodiorites and show similar geochemical features, such as having a high aluminum saturation index and an unfractionated composition. The granites from both provinces show enrichment in light rare earth elements (REE) and negative Eu anomalies. All samples demonstrate characteristic negative Ba, Nb, Ta, Sr and Ti anomalies, and a positive Pb anomaly, when plotted on spidergrams. The Kyaing Tong granites have high and variable initial $^{87}Sr/^{86}Sr$ ratios (0.717735–0.731271), negative ε_{Nd} ($t = 215$ Ma) values (-14.2 to -10.4), and old T_{DM2} ages. Similarly, the Tachileik granites have high and variable initial $^{87}Sr/^{86}Sr$ ratios (0.715336–0.722712), negative ε_{Nd} ($t = 250$ Ma) values (-12.4 to -11.3), and old T_{DM2} ages. Sr–Nd isotope values show that these granites may be generated by mixing of two end-member lithologies: amphibolite and schist of the Lancang Group, which represents the lower crust of the Indochina block. We consider that both the Kyaing Tong and Tachileik granites are of I-type affinity. They were derived from partial melting of the amphibolite and underwent assimilation of schist. Our petrogenetic and zircon U–Pb age data support models that relate the Eastern Province granites to continental arc during the Permian and *syn*-collisional magmatism in the Early Triassic, and the Main Range Province granites to post-collisional magmatism during the Middle to Late Triassic.

1. Introduction

Two of the major granite belts in Southeast Asia are the Main Range and Eastern Province belts that are divided by the Bentong-Raub suture in Malaysia and Chiang Rai Line in Thailand, respectively (*Cobbing* et al., 1986; *Hutchison,* 1977; *Mitchell,* 1977) (Fig. 1). It has been suggested that Eastern Province granitoids are mostly hornblende-bearing I-types that formed above an east-dipping Paleo-Tethys subduction zone, while Main Range Province granitoids are younger and mostly hornblende-free S-types that formed due to crustal thickening following collision between the Sibumasu and Indochina blocks (*Cobbing* et al., 1986; *Schwartz* et al., 1995). Together, these are interpreted to represent the magmatic expression of the closure of the Paleo-Tethys during the Permian and Triassic. However, *Ng* et al. (2015a) argued that direct application of the I- and S-type classification scheme cannot account for many of the characteristics exhibited by Malaysian

* Corresponding author at: State Key Laboratory of Lithospheric Evolution, Institute of Geology and Geophysics, Chinese Academy of Sciences, Beijing 100029, China.
E-mail address: congfeng@mail.cgs.gov.cn (F. Cong).

https://doi.org/10.1016/j.lithos.2020.105895
0024-4937/

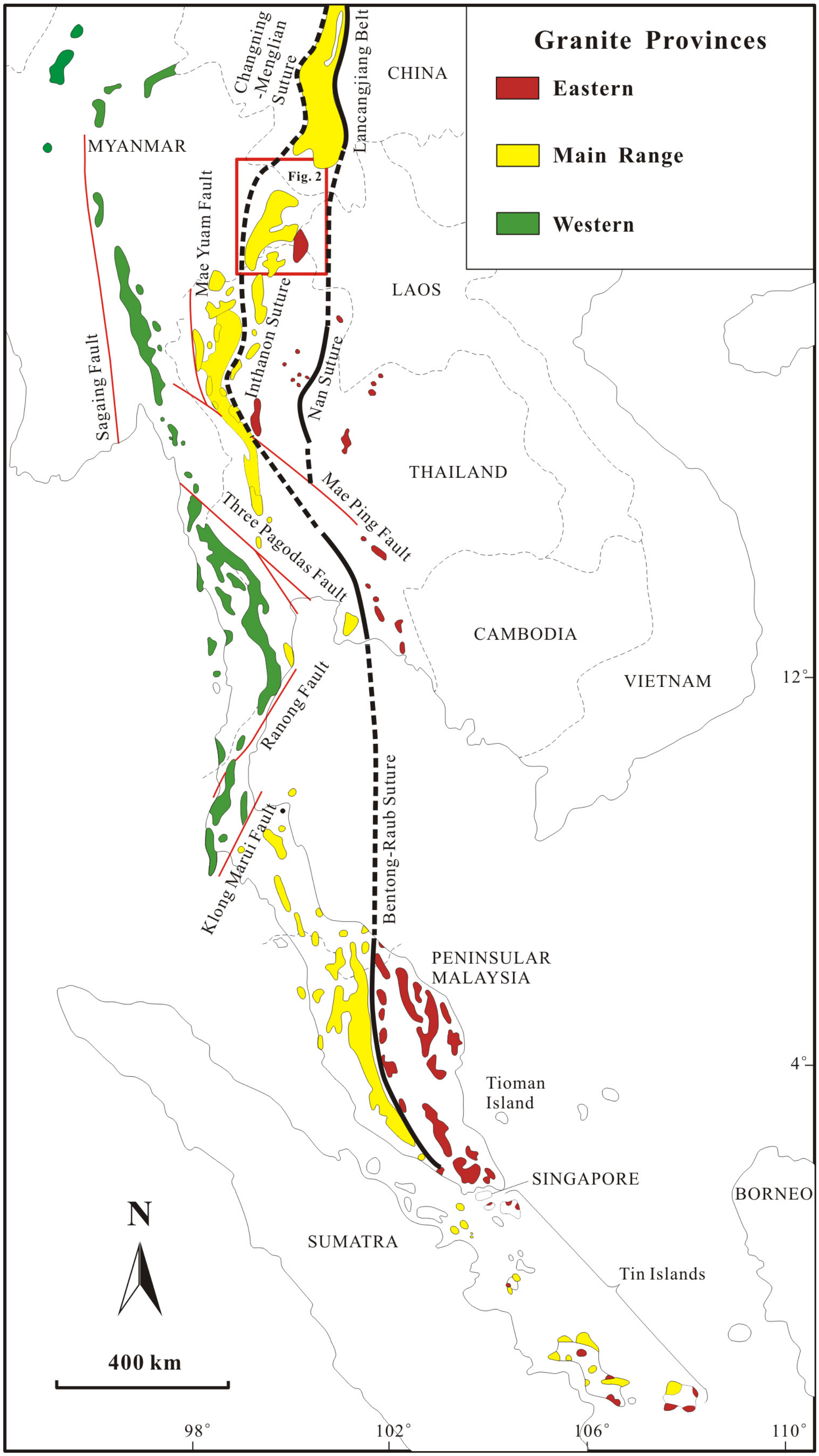

Fig. 1. Simplified map showing the granite belts in mainland Southeast Asia, with major sutures and faults (after Gardiner et al., 2016).

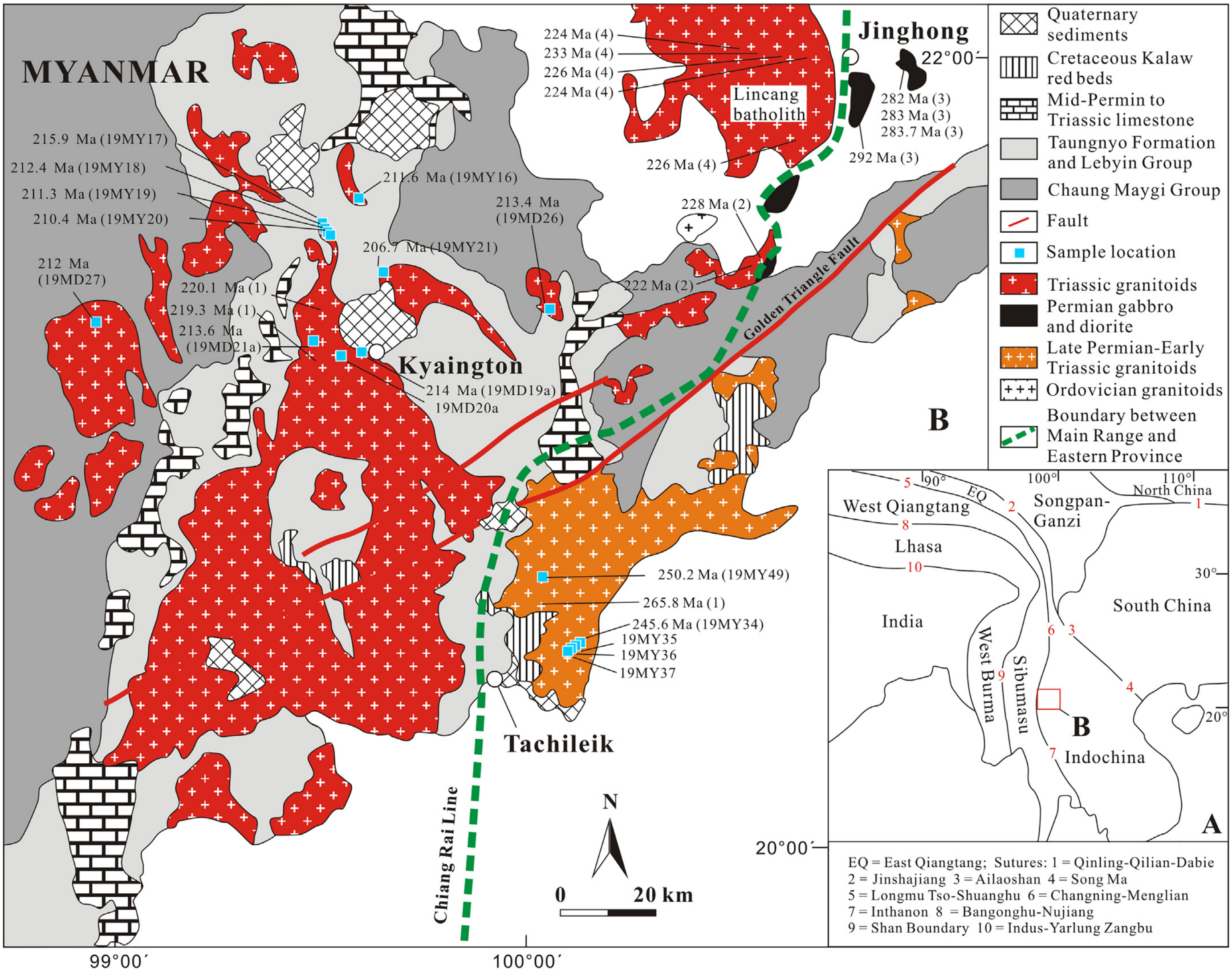

Fig. 2. Simplified geological map and sample locations of the Kyaing Tong and Tachileik granites in eastern Myanmar (after MGS, 2014). The zircon U–Pb ages of different granitoids are from [1] Gardiner et al. (2016), [2] Wang et al. (2015), [3] Hennig et al. (2009), [4] Wang et al. (2014) and this study.

granitoids. Searle et al. (2012), Ghani et al. (2013), and Ng et al. (2015a) suggest that the Malaysian granitoids can be divided by the Bentong-Raub suture zone into an I-type Eastern Province and a transitional I/S-type Main Range Province. Therefore, the petrogenesis of the Main Range Province granites is still a matter of debate. A key issue persists in how the Main Range and Eastern Provinces granitoids petrogenetically relate to each other in the Paleo-Tethys orogenic belt. Recent geochronological and geochemical work has better delineated these belts within Peninsular Malaysia (Liu et al., 2020; Ng et al., 2015a, 2015b; Searle et al., 2012) and the southeastern Tibetan Plateau (Cong et al., 2020; Deng et al., 2018; Dong et al., 2013; Hennig et al., 2009; Peng et al., 2013; Wang et al., 2015). However, in general, due to the lack of reliable geochronology in eastern Myanmar, the Main Range and Eastern Province granite belts in this area are very poorly delineated. The Kyaing Tong and Tachileik granites in eastern Myanmar are important components of the Southeast Asian granite provinces (Gardiner et al., 2016). They provide a unique opportunity for studying the role of crust formation in the Paleo-Tethys orogenic belt and the extension of the Main Range and Eastern Province granite belts in eastern Myanmar. Here we combine zircon U–Pb ages, whole-rock geochemistry, and Sr–Nd isotope data to constrain the petrogenesis of the Kyaing Tong and Tachileik granites, and investigate the extension of the Main Range and Eastern Province granite belts in eastern Myanmar.

2. Geological setting and samples

Mainland Southeast Asia comprises a complex assembly of continental blocks, arc terranes, suture zones, and accreted continental crust. The two major continental masses within mainland Southeast Asia are the Indochina and Sibumasu terranes. The Indochina block is interpreted to have rifted away from Gondwana due to opening of the Paleo-Tethys Ocean during the Early Devonian (Metcalfe, 2011). This block is bounded to the northeast by the Song Ma suture in Vietnam and to the west by the Inthanon-Bentong-Raub Paleo-Tethys suture (Lepvrier et al., 2004) (Fig. 2A). Sibumasu is interpreted to have rifted away from Gondwana during the Late Carboniferous–Early Permian (Metcalfe, 2011). Sibumasu is the accepted term for the contiguous continental block that lies west of the Inthanon-Bentong-Raub Paleo-Tethys suture and extends as far west as the Shan Boundary suture (Metcalfe, 2011) (Fig. 2A). Both continental blocks collided with each other and caused the Indosinian orogeny during the Late Permian–

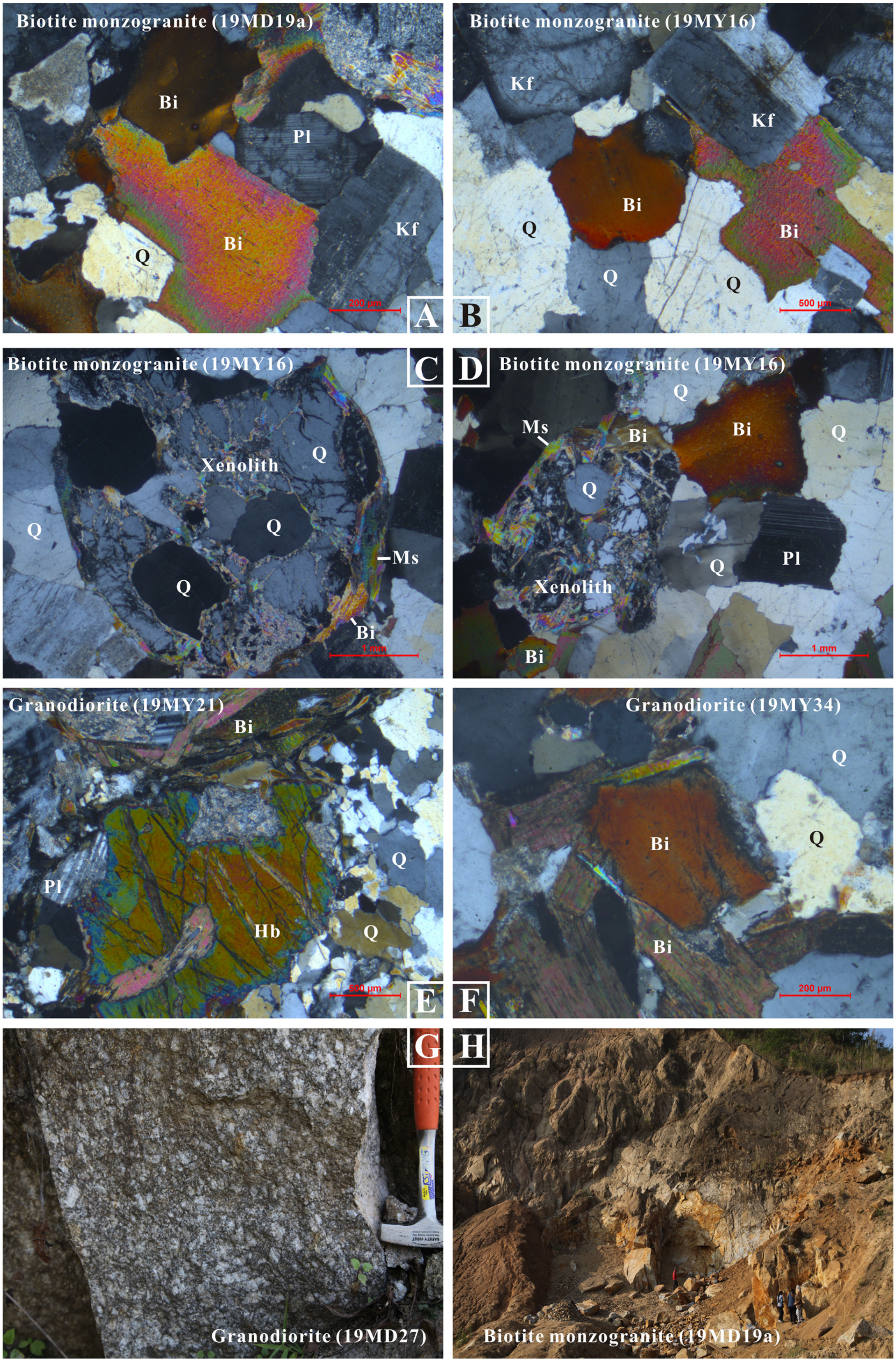

Fig. 3. Textural and petrographic features of the Kyaing Tong and Tachileik granites. (A) and (B) The medium grained biotite monzogranite consists mainly of quartz, alkali-feldspar, plagioclase, and biotite. (C) and (D) The medium grained biotite monzogranite contains a few oval shaped xenoliths of two-mica quartz schists. The xenoliths have a length of 3–6 mm and a width of 2–4 mm. They are made up of quartz, muscovite, and biotite. (E) The medium grained and porphyritic-like granodiorite is made up of plagioclase, alkali-feldspar, quartz, biotite, and hornblende. (F) The medium grained granodiorite consists mainly of quartz, plagioclase, alkali-feldspar, and biotite. Mineral abbreviations: Kf = alkali-feldspar; Pl = Plagioclase; Q = Quartz; Bi = Biotite; Ms. = Muscovite; Hb = Hornblende; Spn = Sphene. (G) The coarse porphyritic-like granodiorite consists mainly of quartz, alkali-feldspar, plagioclase, biotite, and hornblende. (H) The medium grained biotite monzogranite is made up of K-feldspar, plagioclase, quartz, and biotite.

Early Triassic after prolonged subduction of the Paleo-Tethys Ocean, which is recorded by the Changning-Menglian suture in the southeastern Tibetan Plateau, the Inthanon suture in Thailand, and the Bentong-Raub suture in Peninsular Malaysia (Fig. 2A) (*Gardiner* et al., 2016; *Metcalfe,* 2000; *Sone and Metcalfe,* 2008). Within Peninsular Malaysia, the Bentong-Raub suture contains only scattered and limited ophiolite occurrences, serpentinitized ultramafic rocks, and cherts and deep-sea sediments that formed from Middle Devonian to Middle Triassic (*Hutchison,* 1975; *Metcalfe,* 2000; *Sone and Metcalfe,* 2008). The Bentong-Raub suture extends north to the Inthanon suture (*Metcalfe,* 2011), with the Nan-Uttaradit suture of northern Thailand thought to be a back-arc basin (*Metcalfe,* 2013a; *Sone and Metcalfe,* 2008). In northern Thailand, the Inthanon suture has been cut and is offset along numerous Tertiary strike-slip faults, and so becomes harder to trace. The Inthanon suture extends north into southwest China and connects with the Changning-Menglian suture, which contains ophiolitic mélanges, volcanic rocks, shallow-marine carbonates, and deep-sea sedimentary rocks containing substantial amounts of pelagic cherts (*Sone and Metcalfe,* 2008; *Zhong,* 1998).

Geologically, the major tectonic units of Eastern Myanmar can be divided into the Sibumasu terrane in the west and Indochina terrane in the east. *Metcalfe* (2011) suggested that the Inthanon suture represents the delineation between the Sibumasu and Indochina terranes in eastern Myanmar; however, mapping of this suture is extremely difficult due to extensive vegetation and deep lateritic weathering. Study area lies in the east of the Inthanon suture and belongs to the western margin of Indochina terrane (Fig. 2A). The lower crust of the eastern Myanmar is the Precambrian–Early Cambrian Chaung Maygi Group, which consists mainly of mica schists (*MGS,* 2014) (Fig. 2B). The Chaung Maygi Group is the equivalent to the Lancang Group in the southeastern Tibetan Plateau (*Zhong,* 1998). These sequences are overlain by the Carboniferous–Permian clastic sediments of the Taungnyo Formation and the Lebyin Group (*MGS,* 2014) (Fig. 2B). In general, much of the cover is largely comprised of shelf carbonates of Middle Permian to Triassic age (Fig. 2B).

There are three principal granite belts in Southeast Asia (*Cobbing* et al., 1986; *Hutchison,* 1977; *Mitchell,* 1977): (1) the Western Province (Tengchong-Lianghe-Yingjiang in the southeastern Tibetan Plateau, western Myanmar, and southern Thailand), containing mixed I- and S-type granites of Cretaceous age; (2) the Main Range Province (Lincang in the southeastern Tibetan Plateau, northwestern Thailand, and western Malaysia), which is composed of S-type granites of mainly Triassic age; and (3) the Eastern Province (central Thailand and eastern Malaysia), which is dominated by I-type granites of Permian–Triassic age and small I-type plutons of Cretaceous age (Fig. 1). It is generally accepted that the Main Range and Eastern Province granitoids with Permian–Triassic ages are related to subduction and closure of the Paleo-Tethys (*Zhong,* 1998; *Heppe* et al., 2007; *Hennig* et al., 2009; *Jian* et al., 2009; *Searle* et al., 2012; *Dong* et al., 2013; *Peng* et al., 2013; *Wang* et al., 2014; *Ng* et al., 2015a; *Gardiner* et al., 2016; *Wang* et al., 2016; *Qian* et al., 2017; *Deng* et al., 2018; *Cong* et al., 2020; *Liu* et al., 2020). The Cretaceous magmatism that produced the Western Province granitoids is interpreted to be related to subduction of the Neo-Tethys prior to India–Asia collision (*Gardiner* et al., 2015; *Morley,* 2012; *Searle* et al., 2012; *Xu* et al., 2012).

Myanmar has been affected by at least two major Tethyan-related suturing events (*Gardiner* et al., 2018). Closure of the Paleo-Tethys, which likely occurred during the Late Permian to Late Triassic, involved collision of the Sibumasu block with Indochina, and generated the Indosinian Orogeny, whereas the Main Range and Eastern Province granites formed in eastern Myanmar (*Gardiner* et al., 2016; *Macdonald* et al., 1993; *Metcalfe,* 2013a; *Mitchell,* 1977; *Searle* et al., 2012; *Sone and Metcalfe,* 2008). The Mogok-Mandalay-Mergui belt and Wuntho-Popa arc formed in response to the Eocene closure of the Neo-Tethys (*Mitchell* et al., 2007; *Morley,* 2012; *Searle* et al., 2007). In eastern Myanmar, the Kyaing Tong granitoids are even more voluminous than the Tachileik granitoids, and were emplaced as large batholithic bodies up to several thousands of square kilometers in area. The Tachileik pluton is located to the northeast of Tachileik city in eastern Myanmar (Fig. 2B). The Kyaing Tong and Tachileik granitoids were emplaced into Precambrian basement rocks and Paleozoic clastic sediments (*MGS,* 2014).

3. Analytical methods

3.1. Sampling methods and description

Representative rock types were selected from the Kyaing Tong batholith and Tachileik pluton for study in this work (Fig. 2B). The samples were taken from the freshest out crops available at each locality. A schematic map detailing all sample localities and U–Pb ages is shown in Fig. 2B. Lithologic classification of the analyzed granites is based on the visually estimated modes in hand specimens and in thin sections. Eleven granite samples were collected from Kyaing Tong batholith around Kyaing Tong city (Fig. 2B) and consist mainly of medium-grained biotite monzogranite (Fig. 3A, B, C, D and H) and coarse-

Table 1
The lithological characteristics of studied Kyaing Tong and Tachileik granites from eastern Myanmar.

Location	Sample no.	Lithology	Texture	Kf (%)	Pl (%)	Q (%)	Bi (%)	Hb (%)	Accessory minerals
Kyaing Tong	19MD19a	Biotite monzogranite	Medium	30	30	20	20		Mag, Zi, Ap, Mnz
	19MD20a	Biotite monzogranite	Medium	50	25	20	5		Mag, Zi
	19MY16	Biotite monzogranite	Medium	35	25	20	20		Mag, Zi, Ap, Mnz, Xtm
	19MY19	Biotite monzogranite	Fine	35	25	20	20		Mag, Zi
	19MD21a	Biotite monzogranite	Medium	20	45	20	15		Mag, Zi, Ap, Mnz
	19MY17	Biotite monzogranite	Medium	25	40	20	15		Mag, Zi, Mnz, Ap
	19MY18	Biotite monzogranite	Medium	35	30	20	15		Mag, Zi, Ap, Mnz
	19MY20	Biotite monzogranite	Medium	35	30	20	15		Mag, Zi, Mnz
	19MD26	Granodiorite	Coarse porphyritic-like	30	25	20	15	10	Mag, Spn, Ap, Tur, Zi
	19MD27	Granodiorite	Coarse porphyritic-like	35	25	20	10	10	Mag, Zi, Ap, Spn
	19MY21	Granodiorite	Medium porphyritic-like	20	45	20	15	minor	Mag, Spn, Zi, Ap
Tachileik	19MY34	Granodiorite	Fine	10	45	25	20		Mag, Zi, Ap, Mnz, Xtm
	19MY35	Biotite monzogranite	Fine	20	40	20	20		Mag, Zi
	19MY36	Biotite monzogranite	Fine	30	35	20	15		Mag, Zi, Ap
	19MY37	Granodiorite	Fine	15	50	20	15		Mag, Zi, Ap, Mnz
	19MY49	Granodiorite	Medium	15	45	20	20		Mag, Zi

Note: Kf = Alkali feldspar; Pl = Plagioclase; Q = Quartz; Bi = Biotite; Hb = Hornblende; Mag = Magnetite; Zi = Zircon; Ap = Apatite; Spn = sphene; Tourmaline = Tur; Monazite = Mnz; Xtm = Xenotime.

grained granodiorite (Fig. 3E and G). The biotite monzogranites consist mainly of alkali feldspar (20%–50%), plagioclase (25%–45%), quartz (20%), and biotite (5%–20%). The accessory minerals consist of apatite, zircon, monazite, and magnetite. The granodiorites are dominated by alkali feldspar (20%–35%), plagioclase (25%–45%), and quartz (20%) with biotite (10%–15%) and hornblende (< 10%) as the mafic components. The main accessory phases are apatite, zircon, sphene, and magnetite. Five granite samples were collected from Tachileik pluton. They are mainly composed of fine-grained granodiorite and biotite monzogranite (Fig. 3F). The granodiorites are dominated by alkali feldspar (10%–15%), plagioclase (45%–50%), quartz (20%–25%), and biotite (15%–20%). The accessory minerals consist of apatite, zircon, monazite, and magnetite. The biotite monzogranites consist mainly of alkali feldspar (20%–50%), plagioclase (35%–40%), quartz (20%), and biotite (15%–20%). The accessory minerals are dominated by apatite, zircon, and magnetite. Detailed lithological characteristics of the analyzed samples are given in Table 1. In addition, biotite monzogranite sample 19MY16 contains abundant xenoliths of schist comprised mainly of quartz, biotite, and muscovite (Fig. 3C and D). These xenoliths range in size from 2 mm to 5 mm, are rounded in shape, and show sharp contacts with the host granite.

3.2. Major and trace elements analyses

Whole-rock major and trace elements were analyzed at the Institute of Geochemistry, the Chinese Academy of Sciences. Major elements were determined using an X-ray fluorescence spectrometer (XRF). Analytical uncertainties were 3% for major elements. Trace element analyses were performed on a Finnigan MAT ELEMENT inductively coupled plasma mass spectrometer (ICP-MS). Analytical uncertainties were 5% for trace elements with concentrations ≥20 ppm and 10% for those <20 ppm.

3.3. Sr–Nd isotopic analyses

Rb–Sr and Sm–Nd isotopic compositions of whole-rock powders were performed at the Laboratory for Radiogenic Isotope Geochemistry, University of Science and Technology of China. About 150 mg of sample powder was dissolved in a mixture of $HClO_4$ and HF acid solution at 120 °C for 7 days. The solution was dried and re-dissolved in HCl acid solution. Rb–Sr and Sm–Nd isotopic ratios were measured on a Finnigan MAT-262 spectrometer. Analytical precisions are stated as 2 sigma standard errors and more details of the analytical technique are given in *Chen* et al. (2007).

3.4. Zircon U–Pb analyses

The U–Pb analyses of zircon were conducted by LA-ICP-MS at the Wuhan Sample Solution Analytical Technology Co., Ltd., Wuhan, China. Laser sampling was performed using a GeolasPro laser ablation system that consists of a COMPexPro 102 ArF excimer laser (wavelength of 193 nm and maximum energy of 200 mJ) and a MicroLas optical system. An Agilent 7700e ICP-MS instrument was used to acquire ion-signal intensities. Helium was applied as a carrier gas. Argon was used as the make-up gas and mixed with the carrier gas via a T-connector before entering the ICP. The laser spot diameter and frequency were set to 30 μm and 10 Hz in this study. Zircon 91,500 was used as the external standard, zircon GJ-1 was analyzed as an unknown to monitor the data quality and silicate glass NIST 610 was used to optimize the instrument. An Excel-based software ICPMSDataCal was used to perform off-line selection and integration of background and analyzed signals, time-drift correction and quantitative calibration for trace element analysis and U–Pb dating (*Liu* et al., 2008).

4. Results

4.1. U–Pb ages

LA-ICP-MS zircon U–Pb isotope data from 10 granitoids of the Kyaing Tong pluton and two granitoids of the Tachileik pluton are shown in Table 2. Zircons are mostly euhedral, up to 50–250 μm long, and have aspect ratios between 1:1 and 4:1. Oscillatory zoning is common in most crystals. Some zircon grains exhibit inherited cores.

For the biotite monzogranite (Sample 19MD19a), 22 analyses were obtained from 22 zircons. The zircons show variable abundances of Th (68–431 ppm) and U (159–1121 ppm), with Th/U ratios between 0.11 and 0.89. A weighted mean $^{206}Pb/^{238}U$ age of 214 ± 1.4 Ma (Fig. 4A; MSWD = 1.9, 2σ) was calculated from 20 grains and is interpreted as the crystallization age of sample 19MD19a. Spots 6 and 8 yielded significantly older $^{206}Pb/^{238}U$ ages of ca. 882 and 572 Ma, respectively, and so are interpreted to have been obtained from xenocrysts.

Twenty-two analyses were obtained from 22 zircons in biotite monzogranite sample 19MD21a. The zircons show variable abundances of Th (58–905 ppm) and U (221–1666 ppm), with Th/U ratios between 0.05 and 0.73. Twenty-one analyses produced a weighted mean $^{206}Pb/^{238}U$ age of 213.6 ± 1.3 Ma (Fig. 4A; MSWD = 2.0, 2σ), which is interpreted as the crystallization age of sample 19MD21a. Spot 21 yielded a significantly older $^{206}Pb/^{238}U$ age of ca. 550 Ma, which is interpreted to have been obtained from a xenocryst.

Eighteen analyses were obtained from 18 zircons from granodiorite sample 19MD26. Some crystals have a dark color, which indicates a relatively high U content. The zircons show high abundances of Th (426–1408 ppm) and U (667–3117 ppm), and have Th/U ratios between 0.26 and 1. Eighteen analyses yielded a weighted mean $^{206}Pb/^{238}U$ age of 213.4 ± 1.3 Ma (Fig. 4A; MSWD = 2.0, 2σ), which is interpreted as the crystallization age of sample 19MD26.

Fifteen analyses were obtained from 15 zircons in granodiorite sample 19MD27. Many crystals have a dark color (Fig. 4A). The zircons show high abundances of Th (274–1435 ppm) and U (215–2795 ppm), with Th/U ratios between 0.16 and 1.35. Fourteen analyses yielded a weighted mean $^{206}Pb/^{238}U$ age of 212 ± 1.7 Ma (Fig. 4B; MSWD = 2.0, 2σ), which is interpreted as the crystallization age of sample 19MD27. Spot 13 yielded a significantly older $^{206}Pb/^{238}U$ age of ca. 777 Ma, which is interpreted to have been obtained from a xenocryst.

Nineteen analyses were obtained from 19 zircons in biotite monzogranite sample 19MY16. The zircons show variable abundances of Th (45–346 ppm) and U (196–913 ppm), with Th/U ratios between 0.09 and 1.16. All 19 analyses yielded a weighted mean $^{206}Pb/^{238}U$ age of 211.6 ± 1.6 Ma (Fig. 4B; MSWD = 1.9, 2σ), which is interpreted as the crystallization age of sample 19MY16.

Twenty-one analyses were obtained from 21 zircons in biotite monzogranite sample 19MY17. The zircons show variable abundances of Th (69–232 ppm) and U (293–1119 ppm), with Th/U ratios between 0.07 and 0.51. Twenty analyses yielded a weighted mean $^{206}Pb/^{238}U$ age of 215.9 ± 1.2 Ma (Fig. 4B; MSWD = 1.9, 2σ), which is interpreted as the crystallization age of sample 19MY17. Spot 22 yielded a significantly older $^{206}Pb/^{238}U$ age of ca. 849 Ma, which is interpreted to have been obtained from a xenocryst.

Twenty-nine analyses were obtained from 29 zircons in biotite monzogranite sample 19MY18. The zircons show variable abundances of Th (92–450 ppm) and U (207–1624 ppm), with Th/U ratios between 0.1 and 0.56. Twenty-seven analyses yielded a weighted mean $^{206}Pb/^{238}U$ age of 212.4 ± 1.1 Ma (Fig. 4B; MSWD = 1.9, 2σ), which is interpreted as the crystallization age of sample 19MY18. Spots 1 and 10 yielded significantly older $^{206}Pb/^{238}U$ ages of ca. 698 and 247 Ma, respectively, which are interpreted to have been obtained from xenocrysts.

For the biotite monzogranite (Sample 19MY19), 20 analyses were obtained from 20 zircons. The zircons show variable abundances of Th (113–355 ppm) and U (204–1392 ppm), with Th/U ratios between

Table 2
LA-ICP-MS zircon U–Pb data for Kyaing Tong and Tachileik granites from eastern Myanmar.

Spot No.	Th (ppm)	U (ppm)	Th/U	Pb (ppm)	Isotopic ratios						Isotopic ages (Ma)					
					$^{207}Pb/^{206}Pb$	±1σ	$^{207}Pb/^{235}U$	±1σ	$^{206}Pb/^{238}U$	±1σ	$^{207}Pb/^{206}Pb$	±1σ	$^{207}Pb/^{235}U$	±1σ	$^{206}Pb/^{238}U$	±1σ
19MD19a																
1	327	700	0.47	27	0.0525	0.0017	0.2435	0.0078	0.0335	0.0003	306	81	221	6	213	2
2	139	945	0.15	34	0.0514	0.0013	0.2459	0.0061	0.0346	0.0003	257	62	223	5	219	2
3	85	409	0.21	15	0.0510	0.0018	0.2467	0.0087	0.0348	0.0003	243	80	224	7	221	2
4	192	503	0.38	20	0.0514	0.0018	0.2447	0.0083	0.0345	0.0004	257	84	222	7	218	2
5	147	512	0.29	19	0.0503	0.0019	0.2368	0.0090	0.0341	0.0004	209	89	216	7	216	2
6	74	309	0.24	50	0.0710	0.0017	1.4436	0.0338	0.1466	0.0011	967	49	907	14	882	6
7	174	613	0.28	23	0.0503	0.0015	0.2400	0.0075	0.0344	0.0003	209	38	218	6	218	2
8	136	459	0.30	47	0.0615	0.0015	0.7915	0.0211	0.0928	0.0012	657	53	592	12	572	7
9	341	437	0.78	18	0.0504	0.0019	0.2333	0.0084	0.0335	0.0003	213	89	213	7	213	2
10	161	836	0.19	30	0.0512	0.0016	0.2368	0.0071	0.0334	0.0003	256	70	216	6	212	2
11	68	602	0.11	21	0.0507	0.0017	0.2348	0.0077	0.0335	0.0003	233	76	214	6	212	2
12	124	671	0.19	25	0.0513	0.0016	0.2398	0.0076	0.0337	0.0003	254	68	218	6	214	2
13	138	644	0.21	24	0.0500	0.0016	0.2313	0.0074	0.0333	0.0003	198	106	211	6	211	2
14	244	275	0.89	12	0.0504	0.0015	0.2323	0.0071	0.0335	0.0004	213	69	212	6	212	2
15	103	159	0.65	6	0.0473	0.0018	0.2180	0.0082	0.0334	0.0004	65	85	200	7	212	2
16	210	482	0.43	19	0.0514	0.0010	0.2369	0.0048	0.0335	0.0004	261	46	216	4	212	2
17	249	883	0.28	32	0.0524	0.0009	0.2438	0.0049	0.0337	0.0005	306	5	222	4	214	3
18	175	253	0.69	11	0.0531	0.0032	0.2424	0.0082	0.0337	0.0003	332	137	220	7	214	2
19	431	978	0.44	37	0.0494	0.0008	0.2273	0.0048	0.0333	0.0004	165	44	208	4	211	3
20	397	632	0.63	26	0.0509	0.0011	0.2341	0.0052	0.0333	0.0004	239	50	214	4	211	2
21	268	471	0.57	19	0.0517	0.0013	0.2407	0.0062	0.0338	0.0004	333	57	219	5	215	2
22	279	1121	0.25	42	0.0495	0.0008	0.2280	0.0038	0.0334	0.0003	172	39	209	3	212	2
Spot No.	Th (ppm)	U (ppm)	Th/U	Pb (ppm)	Isotopic ratios						Isotopic ages (Ma)					
					$^{207}Pb/^{206}Pb$	±1σ	$^{207}Pb/^{235}U$	±1σ	$^{206}Pb/^{238}U$	±1σ	$^{207}Pb/^{206}Pb$	±1σ	$^{207}Pb/^{235}U$	±1σ	$^{206}Pb/^{238}U$	±1σ
19MD21a																
1	162	565	0.29	21	0.0511	0.0020	0.2388	0.0088	0.0339	0.0004	256	82	217	7	215	2
2	88	338	0.26	13	0.0521	0.0020	0.2420	0.0089	0.0337	0.0004	287	87	220	7	214	2
3	89	1666	0.05	59	0.0516	0.0013	0.2485	0.0075	0.0345	0.0005	265	59	225	6	218	3
4	196	520	0.38	20	0.0503	0.0018	0.2356	0.0082	0.0338	0.0004	209	88	215	7	214	2
5	241	845	0.28	32	0.0507	0.0014	0.2420	0.0070	0.0343	0.0003	228	69	220	6	218	2
6	81	1038	0.08	37	0.0507	0.0014	0.2409	0.0066	0.0342	0.0003	228	61	219	5	217	2
7	116	678	0.17	25	0.0512	0.0015	0.2434	0.0070	0.0343	0.0003	250	64	221	6	218	2
8	392	752	0.52	29	0.0502	0.0017	0.2332	0.0076	0.0335	0.0003	206	76	213	6	213	2
9	86	621	0.14	23	0.0502	0.0018	0.2370	0.0084	0.0341	0.0003	211	81	216	7	216	2
10	598	1058	0.57	43	0.0530	0.0015	0.2470	0.0072	0.0336	0.0003	328	65	224	6	213	2
11	153	353	0.43	14	0.0544	0.0024	0.2577	0.0104	0.0342	0.0004	387	96	233	8	217	3
14	905	1234	0.73	51	0.0516	0.0020	0.2386	0.0064	0.0331	0.0003	333	95	217	5	210	2
15	120	221	0.54	9	0.0526	0.0027	0.2463	0.0120	0.0341	0.0004	322	119	224	10	216	3
16	273	534	0.51	21	0.0535	0.0018	0.2447	0.0082	0.0330	0.0003	350	50	222	7	209	2
17	69	845	0.08	29	0.0519	0.0017	0.2375	0.0076	0.0330	0.0003	280	74	216	6	209	2
18	58	406	0.14	15	0.0499	0.0020	0.2344	0.0090	0.0339	0.0004	191	94	214	7	215	3
19	227	553	0.41	21	0.0555	0.0023	0.2540	0.0103	0.0331	0.0004	432	88	230	8	210	2
20	296	940	0.31	36	0.0512	0.0015	0.2397	0.0069	0.0337	0.0003	250	64	218	6	214	2
21	125	296	0.42	29	0.0568	0.0017	0.7093	0.0274	0.0890	0.0020	487	67	544	16	550	12
22	127	357	0.36	13	0.0536	0.0022	0.2463	0.0103	0.0330	0.0003	367	97	224	8	210	2
23	163	399	0.41	16	0.0495	0.0021	0.2343	0.0097	0.0342	0.0003	172	128	214	8	217	2
24	179	377	0.48	15	0.0518	0.0020	0.2414	0.0093	0.0336	0.0003	280	89	220	8	213	2
Spot No.	Th (ppm)	U (ppm)	Th/U	Pb (ppm)	Isotopic ratios						Isotopic ages (Ma)					
					$^{207}Pb/^{206}Pb$	±1σ	$^{207}Pb/^{235}U$	±1σ	$^{206}Pb/^{238}U$	±1σ	$^{207}Pb/^{206}Pb$	±1σ	$^{207}Pb/^{235}U$	±1σ	$^{206}Pb/^{238}U$	±1σ
19MD26																
1	496	1932	0.26	71	0.0521	0.0014	0.2432	0.0063	0.0337	0.0003	300	59	221	5	214	2
2	1408	1583	0.89	69	0.0536	0.0023	0.2551	0.0073	0.0339	0.0003	367	96	231	6	215	2
3	1022	3117	0.33	149	0.0492	0.0051	0.2342	0.0237	0.0339	0.0003	167	217	214	20	215	2
4	667	667	1.00	31	0.0500	0.0020	0.2350	0.0092	0.0339	0.0003	198	93	214	8	215	2
5	704	1544	0.46	68	0.0496	0.0020	0.2369	0.0094	0.0345	0.0003	176	127	216	8	219	2
6	682	839	0.81	36	0.0523	0.0016	0.2404	0.0069	0.0332	0.0003	298	69	219	6	211	2
8	642	1177	0.55	47	0.0543	0.0014	0.2526	0.0063	0.0335	0.0003	383	59	229	5	213	2
9	587	2085	0.28	94	0.0495	0.0020	0.2356	0.0094	0.0343	0.0003	169	94	215	8	218	2
11	952	1662	0.57	66	0.0487	0.0012	0.2274	0.0055	0.0336	0.0003	200	59	208	5	213	2
12	481	873	0.55	36	0.0515	0.0020	0.2379	0.0099	0.0331	0.0003	261	91	217	8	210	2
13	475	1253	0.38	48	0.0547	0.0016	0.2564	0.0069	0.0339	0.0003	398	58	232	6	215	2
14	638	1082	0.59	43	0.0498	0.0015	0.2323	0.0069	0.0337	0.0003	183	66	212	6	214	2
15	448	1428	0.31	52	0.0514	0.0014	0.2368	0.0063	0.0332	0.0003	257	61	216	5	211	2
16	592	1370	0.43	52	0.0491	0.0012	0.2265	0.0054	0.0334	0.0003	150	55	207	4	212	2
17	426	674	0.63	27	0.0523	0.0016	0.2453	0.0074	0.0340	0.0003	298	68	223	6	215	2
18	1391	1543	0.90	65	0.0520	0.0014	0.2394	0.0062	0.0332	0.0003	287	56	218	5	211	2
20	667	1316	0.51	51	0.0491	0.0018	0.2270	0.0072	0.0333	0.0003	154	79	208	6	211	2
23	867	1733	0.50	95	0.0533	0.0045	0.2495	0.0211	0.0334	0.0003	339	162	226	17	212	2

Spot No.	Th (ppm)	U (ppm)	Th/U	Pb (ppm)	Isotopic ratios						Isotopic ages (Ma)					
					$^{207}Pb/^{206}Pb$	±1σ	$^{207}Pb/^{235}U$	±1σ	$^{206}Pb/^{238}U$	±1σ	$^{207}Pb/^{206}Pb$	±1σ	$^{207}Pb/^{235}U$	±1σ	$^{206}Pb/^{238}U$	±1σ
19MD27																
1	444	1720	0.26	63	0.0494	0.0011	0.2291	0.0053	0.0334	0.0003	169	49	209	4	212	2
2	492	667	0.74	28	0.0505	0.0015	0.2346	0.0067	0.0336	0.0003	220	69	214	6	213	2
3	782	1327	0.59	53	0.0514	0.0014	0.2351	0.0064	0.0330	0.0003	257	63	214	5	209	2
4	420	1734	0.24	63	0.0509	0.0013	0.2345	0.0058	0.0333	0.0003	239	53	214	5	211	2
5	274	1723	0.16	62	0.0502	0.0012	0.2364	0.0055	0.0340	0.0003	211	54	215	5	216	2
6	351	2214	0.16	80	0.0515	0.0010	0.2430	0.0051	0.0341	0.0004	261	46	221	4	216	2
7	468	1308	0.36	49	0.0501	0.0014	0.2300	0.0063	0.0332	0.0003	198	31	210	5	210	2
8	1435	1903	0.75	78	0.0506	0.0013	0.2307	0.0061	0.0329	0.0003	233	59	211	5	209	2
9	461	1503	0.31	57	0.0494	0.0016	0.2261	0.0079	0.0330	0.0003	169	78	207	7	209	2
10	498	2309	0.22	82	0.0507	0.0013	0.2325	0.0058	0.0331	0.0003	228	57	212	5	210	2
11	400	771	0.52	30	0.0500	0.0014	0.2298	0.0067	0.0332	0.0004	195	67	210	6	211	2
12	500	753	0.66	30	0.0512	0.0016	0.2364	0.0074	0.0334	0.0003	256	70	215	6	212	2
13	291	215	1.35	39	0.0675	0.0018	1.1961	0.0352	0.1282	0.0020	854	56	799	16	777	12
14	324	1085	0.30	41	0.0517	0.0015	0.2453	0.0074	0.0343	0.0003	272	64	223	6	217	2
15	479	2795	0.17	100	0.0465	0.0013	0.2192	0.0067	0.0342	0.0004	33	54	201	6	217	3

Spot No.	Th (ppm)	U (ppm)	Th/U	Pb (ppm)	Isotopic ratios						Isotopic ages (Ma)					
					$^{207}Pb/^{206}Pb$	±1σ	$^{207}Pb/^{235}U$	±1σ	$^{206}Pb/^{238}U$	±1σ	$^{207}Pb/^{206}Pb$	±1σ	$^{207}Pb/^{235}U$	±1σ	$^{206}Pb/^{238}U$	±1σ
19MY16																
1	135	403	0.34	15	0.0520	0.0019	0.2403	0.0088	0.0336	0.0004	287	79	219	7	213	2
2	45	515	0.09	18	0.0533	0.0019	0.2448	0.0090	0.0333	0.0004	339	83	222	7	211	2
3	346	298	1.16	14	0.0506	0.0024	0.2333	0.0109	0.0335	0.0004	233	109	213	9	212	2
4	252	399	0.63	15	0.0487	0.0020	0.2187	0.0086	0.0326	0.0004	200	99	201	7	207	2
6	195	416	0.47	16	0.0533	0.0019	0.2395	0.0085	0.0327	0.0004	343	81	218	7	208	3
7	105	495	0.21	18	0.0526	0.0022	0.2496	0.0106	0.0343	0.0005	322	94	226	9	217	3
8	161	258	0.62	10	0.0558	0.0024	0.2512	0.0106	0.0327	0.0004	443	129	228	9	207	2
9	113	238	0.47	9	0.0519	0.0023	0.2422	0.0104	0.0342	0.0005	280	100	220	8	217	3
10	153	487	0.31	18	0.0511	0.0021	0.2306	0.0091	0.0327	0.0004	256	97	211	8	207	2
11	101	339	0.30	13	0.0545	0.0024	0.2499	0.0106	0.0334	0.0004	391	94	226	9	211	3
12	111	196	0.57	8	0.0492	0.0028	0.2309	0.0129	0.0341	0.0006	167	131	211	11	216	3
13	151	308	0.49	12	0.0556	0.0021	0.2546	0.0099	0.0331	0.0004	435	85	230	8	210	2
14	213	551	0.39	21	0.0512	0.0018	0.2394	0.0085	0.0337	0.0004	250	80	218	7	214	3
15	272	913	0.30	34	0.0510	0.0014	0.2335	0.0067	0.0330	0.0003	243	65	213	5	209	2
16	202	610	0.33	23	0.0522	0.0017	0.2475	0.0080	0.0343	0.0004	300	74	225	7	218	2
17	162	407	0.40	16	0.0501	0.0020	0.2306	0.0090	0.0335	0.0004	198	99	211	7	212	2
18	193	445	0.43	17	0.0523	0.0020	0.2386	0.0089	0.0330	0.0004	298	90	217	7	210	2
19	60	433	0.14	16	0.0527	0.0020	0.2448	0.0091	0.0337	0.0004	317	119	222	7	214	2
20	131	418	0.31	16	0.0514	0.0022	0.2382	0.0100	0.0337	0.0004	261	100	217	8	214	2

Spot No.	Th (ppm)	U (ppm)	Th/U	Pb (ppm)	Isotopic ratios						Isotopic ages (Ma)					
					$^{207}Pb/^{206}Pb$	±1σ	$^{207}Pb/^{235}U$	±1σ	$^{206}Pb/^{238}U$	±1σ	$^{207}Pb/^{206}Pb$	±1σ	$^{207}Pb/^{235}U$	±1σ	$^{206}Pb/^{238}U$	±1σ
19MY17																
2	146	433	0.34	16	0.0524	0.0020	0.2509	0.0093	0.0346	0.0003	302	85	227	8	219	2
3	184	1081	0.17	38	0.0508	0.0014	0.2363	0.0062	0.0336	0.0003	232	66	215	5	213	2
4	170	451	0.38	17	0.0524	0.0020	0.2469	0.0091	0.0341	0.0003	302	85	224	7	216	2
5	96	698	0.14	25	0.0516	0.0015	0.2444	0.0067	0.0342	0.0003	333	60	222	5	217	2
6	232	713	0.33	26	0.0497	0.0016	0.2356	0.0081	0.0341	0.0004	189	74	215	7	216	2
8	125	939	0.13	33	0.0516	0.0015	0.2436	0.0071	0.0340	0.0003	333	73	221	6	216	2
10	82	759	0.11	26	0.0481	0.0015	0.2291	0.0074	0.0342	0.0004	106	81	209	6	217	2
11	118	1119	0.11	38	0.0507	0.0013	0.2363	0.0063	0.0336	0.0003	228	61	215	5	213	2
12	158	824	0.19	29	0.0508	0.0014	0.2381	0.0064	0.0338	0.0003	232	66	217	5	214	2
13	149	293	0.51	11	0.0508	0.0022	0.2381	0.0104	0.0339	0.0004	232	102	217	9	215	2
14	69	1024	0.07	34	0.0499	0.0014	0.2306	0.0064	0.0333	0.0003	191	63	211	5	211	2
15	101	1025	0.10	36	0.0501	0.0013	0.2407	0.0060	0.0348	0.0003	198	27	219	5	220	2
16	133	988	0.13	35	0.0506	0.0014	0.2392	0.0065	0.0342	0.0003	233	60	218	5	217	2
17	145	726	0.20	26	0.0489	0.0015	0.2303	0.0073	0.0340	0.0003	146	72	210	6	216	2
18	98	708	0.14	25	0.0538	0.0016	0.2484	0.0074	0.0335	0.0003	361	64	225	6	213	2
19	141	384	0.37	14	0.0534	0.0021	0.2535	0.0094	0.0345	0.0003	346	89	229	8	219	2
20	171	563	0.30	21	0.0525	0.0017	0.2472	0.0082	0.0341	0.0003	309	76	224	7	216	2
21	132	1027	0.13	36	0.0517	0.0014	0.2451	0.0069	0.0343	0.0003	333	69	223	6	218	2
22	129	592	0.22	87	0.0708	0.0014	1.3809	0.0366	0.1408	0.0025	954	36	881	16	849	14
23	131	698	0.19	25	0.0478	0.0015	0.2255	0.0071	0.0343	0.0003	87	74	207	6	217	2
24	180	556	0.32	21	0.0538	0.0017	0.2576	0.0080	0.0348	0.0003	361	72	233	6	221	2

Spot No.	Th (ppm)	U (ppm)	Th/U	Pb (ppm)	Isotopic ratios						Isotopic ages (Ma)					
					$^{207}Pb/^{206}Pb$	±1σ	$^{207}Pb/^{235}U$	±1σ	$^{206}Pb/^{238}U$	±1σ	$^{207}Pb/^{206}Pb$	±1σ	$^{207}Pb/^{235}U$	±1σ	$^{206}Pb/^{238}U$	±1σ
19MY18																
1	204	374	0.54	51	0.0619	0.0016	0.9796	0.0245	0.1143	0.0010	672	54	693	13	698	6
2	183	626	0.29	24	0.0511	0.0017	0.2394	0.0077	0.0340	0.0003	256	78	218	6	215	2
3	250	1091	0.23	40	0.0514	0.0013	0.2380	0.0061	0.0335	0.0003	257	59	217	5	212	2
4	117	829	0.14	29	0.0504	0.0015	0.2288	0.0063	0.0329	0.0003	213	67	209	5	209	2
5	318	867	0.37	33	0.0505	0.0013	0.2329	0.0060	0.0334	0.0003	220	56	213	5	212	2

Table 2 (*continued*)

Spot No.	Th (ppm)	U (ppm)	Th/U	Pb (ppm)	Isotopic ratios						Isotopic ages (Ma)					
					$^{207}Pb/^{206}Pb$	±1σ	$^{207}Pb/^{235}U$	±1σ	$^{206}Pb/^{238}U$	±1σ	$^{207}Pb/^{206}Pb$	±1σ	$^{207}Pb/^{235}U$	±1σ	$^{206}Pb/^{238}U$	±1σ
6	129	997	0.13	35	0.0528	0.0017	0.2405	0.0078	0.0329	0.0003	317	66	219	6	209	2
7	150	806	0.19	29	0.0527	0.0016	0.2400	0.0076	0.0329	0.0004	317	66	218	6	209	2
8	275	772	0.36	30	0.0521	0.0021	0.2492	0.0103	0.0345	0.0004	300	95	226	8	218	2
9	311	899	0.35	34	0.0515	0.0017	0.2333	0.0075	0.0328	0.0003	261	79	213	6	208	2
10	195	645	0.30	27	0.0500	0.0017	0.2688	0.0092	0.0390	0.0005	195	75	242	7	247	3
11	450	1125	0.40	43	0.0516	0.0015	0.2390	0.0072	0.0334	0.0003	333	67	218	6	212	2
12	168	828	0.20	30	0.0495	0.0015	0.2293	0.0069	0.0335	0.0003	172	70	210	6	212	2
13	418	1251	0.33	47	0.0515	0.0014	0.2406	0.0066	0.0337	0.0003	261	55	219	5	214	2
14	278	1192	0.23	43	0.0518	0.0014	0.2388	0.0063	0.0334	0.0003	276	63	217	5	212	2
15	175	516	0.34	20	0.0541	0.0019	0.2493	0.0084	0.0335	0.0003	376	80	226	7	212	2
16	166	1624	0.10	56	0.0522	0.0013	0.2401	0.0061	0.0332	0.0003	295	56	219	5	211	2
17	116	207	0.56	9	0.0559	0.0037	0.2644	0.0166	0.0344	0.0005	456	146	238	13	218	3
18	155	470	0.33	18	0.0512	0.0019	0.2421	0.0087	0.0344	0.0004	256	89	220	7	218	2
19	173	642	0.27	23	0.0509	0.0018	0.2306	0.0080	0.0329	0.0003	235	81	211	7	209	2
20	92	864	0.11	28	0.0516	0.0019	0.2442	0.0111	0.0335	0.0006	333	82	222	9	212	4
21	231	491	0.47	19	0.0529	0.0026	0.2431	0.0075	0.0333	0.0003	324	109	221	6	211	2
22	191	1147	0.17	39	0.0508	0.0009	0.2381	0.0064	0.0338	0.0006	232	41	217	5	214	4
23	167	218	0.77	10	0.0508	0.0022	0.2354	0.0080	0.0337	0.0004	235	98	215	7	214	2
24	124	337	0.37	13	0.0514	0.0016	0.2370	0.0072	0.0335	0.0003	257	70	216	6	213	2
25	196	472	0.42	18	0.0528	0.0013	0.2463	0.0066	0.0336	0.0003	320	56	224	5	213	2
26	210	721	0.29	26	0.0520	0.0017	0.2415	0.0067	0.0335	0.0005	287	79	220	5	212	3
27	300	1021	0.29	37	0.0498	0.0008	0.2295	0.0051	0.0334	0.0005	183	37	210	4	212	3
28	266	515	0.52	21	0.0522	0.0013	0.2475	0.0065	0.0343	0.0003	300	57	225	5	218	2
29	135	326	0.41	13	0.0512	0.0014	0.2380	0.0063	0.0338	0.0003	256	61	217	5	214	2
Spot No.	Th (ppm)	U (ppm)	Th/U	Pb (ppm)	Isotopic ratios						Isotopic ages (Ma)					
					$^{207}Pb/^{206}Pb$	±1σ	$^{207}Pb/^{235}U$	±1σ	$^{206}Pb/^{238}U$	±1σ	$^{207}Pb/^{206}Pb$	±1σ	$^{207}Pb/^{235}U$	±1σ	$^{206}Pb/^{238}U$	±1σ
19MY19																
1	208	583	0.36	21	0.0540	0.0017	0.2507	0.0079	0.0336	0.0003	372	70	227	6	213	2
3	168	346	0.49	13	0.0521	0.0021	0.2423	0.0092	0.0340	0.0003	287	91	220	8	215	2
4	150	865	0.17	30	0.0524	0.0014	0.2394	0.0062	0.0331	0.0003	306	61	218	5	210	2
5	174	1042	0.17	37	0.0477	0.0012	0.2218	0.0056	0.0337	0.0003	83	56	203	5	213	2
6	355	900	0.39	33	0.0521	0.0014	0.2375	0.0064	0.0330	0.0003	287	58	216	5	209	2
7	274	746	0.37	27	0.0514	0.0015	0.2341	0.0070	0.0329	0.0003	257	69	214	6	209	2
8	145	1072	0.14	37	0.0491	0.0013	0.2267	0.0062	0.0333	0.0003	154	58	208	5	211	2
9	140	1021	0.14	36	0.0495	0.0014	0.2323	0.0066	0.0339	0.0003	172	67	212	5	215	2
10	187	790	0.24	28	0.0507	0.0016	0.2334	0.0068	0.0334	0.0003	228	72	213	6	212	2
11	113	204	0.56	8	0.0497	0.0026	0.2293	0.0125	0.0332	0.0004	189	124	210	10	210	3
12	163	872	0.19	30	0.0508	0.0014	0.2302	0.0063	0.0328	0.0003	232	65	210	5	208	2
13	235	543	0.43	20	0.0503	0.0015	0.2302	0.0072	0.0330	0.0003	209	40	210	6	209	2
14	175	1008	0.17	35	0.0513	0.0013	0.2338	0.0059	0.0330	0.0003	254	59	213	5	209	2
17	148	805	0.18	28	0.0480	0.0014	0.2216	0.0065	0.0334	0.0003	102	72	203	5	212	2
18	196	624	0.31	23	0.0474	0.0015	0.2233	0.0071	0.0341	0.0003	78	65	205	6	216	2
20	128	369	0.35	14	0.0516	0.0022	0.2391	0.0097	0.0337	0.0004	333	98	218	8	213	2
21	273	774	0.35	28	0.0502	0.0012	0.2313	0.0058	0.0333	0.0003	211	56	211	5	211	2
22	175	1211	0.14	42	0.0486	0.0012	0.2217	0.0055	0.0330	0.0003	128	61	203	5	209	2
23	177	1392	0.13	48	0.0487	0.0012	0.2231	0.0052	0.0331	0.0003	132	56	204	4	210	2
24	195	544	0.36	20	0.0518	0.0018	0.2419	0.0083	0.0337	0.0003	276	80	220	7	214	2
Spot No.	Th (ppm)	U (ppm)	Th/U	Pb (ppm)	Isotopic ratios						Isotopic ages (Ma)					
					$^{207}Pb/^{206}Pb$	±1σ	$^{207}Pb/^{235}U$	±1σ	$^{206}Pb/^{238}U$	±1σ	$^{207}Pb/^{206}Pb$	±1σ	$^{207}Pb/^{235}U$	±1σ	$^{206}Pb/^{238}U$	±1σ
19MY20																
1	116	685	0.17	24	0.0479	0.0013	0.2234	0.0059	0.0337	0.0003	98	68	205	5	214	2
2	141	718	0.20	25	0.0479	0.0015	0.2216	0.0066	0.0335	0.0003	95	68	203	6	212	2
3	194	1042	0.19	41	0.0514	0.0015	0.3140	0.0155	0.0433	0.0014	261	69	277	12	273	9
4	473	1104	0.43	82	0.0544	0.0012	0.4751	0.0126	0.0631	0.0011	387	48	395	9	394	6
5	86	667	0.13	23	0.0477	0.0014	0.2140	0.0058	0.0326	0.0003	83	69	197	5	207	2
6	211	890	0.24	33	0.0530	0.0016	0.2490	0.0072	0.0341	0.0003	332	69	226	6	216	2
7	66	672	0.10	24	0.0497	0.0015	0.2321	0.0072	0.0337	0.0003	183	72	212	6	214	2
8	154	1564	0.10	54	0.0497	0.0012	0.2237	0.0051	0.0326	0.0002	183	54	205	4	207	1
9	75	436	0.17	15	0.0504	0.0018	0.2294	0.0081	0.0330	0.0003	217	81	210	7	209	2
10	212	775	0.27	28	0.0516	0.0015	0.2360	0.0069	0.0332	0.0003	333	73	215	6	210	2
11	133	789	0.17	29	0.0526	0.0014	0.2445	0.0065	0.0337	0.0003	322	63	222	5	213	2
12	120	868	0.14	30	0.0520	0.0013	0.2356	0.0057	0.0328	0.0003	287	57	215	5	208	2
13	146	298	0.49	11	0.0521	0.0022	0.2352	0.0090	0.0328	0.0004	300	98	215	7	208	2
14	213	833	0.26	31	0.0508	0.0018	0.2366	0.0082	0.0337	0.0003	232	80	216	7	214	2
15	152	537	0.28	20	0.0508	0.0011	0.2318	0.0050	0.0331	0.0003	235	50	212	4	210	2
16	155	505	0.31	18	0.0503	0.0022	0.2314	0.0067	0.0330	0.0004	209	102	211	6	209	2
17	102	264	0.39	10	0.0529	0.0019	0.2374	0.0075	0.0327	0.0004	324	114	216	6	208	2
18	157	1263	0.12	42	0.0512	0.0009	0.2345	0.0068	0.0329	0.0006	250	45	214	6	209	4
19	140	520	0.27	18	0.0503	0.0012	0.2269	0.0056	0.0327	0.0004	209	56	208	5	208	2
20	207	860	0.24	34	0.0494	0.0013	0.2224	0.0060	0.0328	0.0005	169	61	204	5	208	3

(continued on next page)

Table 2 (*continued*)

Spot No.	Th (ppm)	U (ppm)	Th/U	Pb (ppm)	Isotopic ratios						Isotopic ages (Ma)					
					$^{207}Pb/^{206}Pb$	±1σ	$^{207}Pb/^{235}U$	±1σ	$^{206}Pb/^{238}U$	±1σ	$^{207}Pb/^{206}Pb$	±1σ	$^{207}Pb/^{235}U$	±1σ	$^{206}Pb/^{238}U$	±1σ
21	131	630	0.21	22	0.0513	0.0010	0.2324	0.0049	0.0329	0.0004	257	46	212	4	209	3
22	313	574	0.55	22	0.0493	0.0010	0.2244	0.0046	0.0330	0.0004	165	46	206	4	209	2

Spot No.	Th (ppm)	U (ppm)	Th/U	Pb (ppm)	Isotopic ratios						Isotopic ages (Ma)					
					$^{207}Pb/^{206}Pb$	±1σ	$^{207}Pb/^{235}U$	±1σ	$^{206}Pb/^{238}U$	±1σ	$^{207}Pb/^{206}Pb$	±1σ	$^{207}Pb/^{235}U$	±1σ	$^{206}Pb/^{238}U$	±1σ
19MY21																
1	120	682	0.18	24	0.0531	0.0016	0.2413	0.0076	0.0327	0.0003	345	103	220	6	208	2
2	191	610	0.31	22	0.0521	0.0018	0.2316	0.0077	0.0321	0.0003	300	78	211	6	204	2
3	261	1005	0.26	35	0.0528	0.0014	0.2374	0.0063	0.0325	0.0003	320	66	216	5	206	2
4	394	2596	0.15	90	0.0512	0.0011	0.2315	0.0053	0.0326	0.0002	250	52	211	4	207	1
5	211	509	0.42	19	0.0524	0.0019	0.2402	0.0091	0.0331	0.0003	306	81	219	7	210	2
6	582	1798	0.32	65	0.0520	0.0013	0.2327	0.0059	0.0324	0.0003	283	56	212	5	206	2
7	193	698	0.28	25	0.0490	0.0017	0.2232	0.0082	0.0330	0.0003	150	85	205	7	209	2
8	617	1488	0.41	56	0.0532	0.0013	0.2397	0.0063	0.0326	0.0003	345	57	218	5	207	2
9	201	447	0.45	17	0.0500	0.0019	0.2250	0.0083	0.0328	0.0004	195	87	206	7	208	2
10	181	399	0.45	15	0.0480	0.0021	0.2195	0.0096	0.0333	0.0003	98	113	201	8	211	2
11	156	321	0.49	12	0.0485	0.0021	0.2131	0.0091	0.0320	0.0004	120	104	196	8	203	2
12	185	391	0.47	15	0.0512	0.0020	0.2286	0.0088	0.0323	0.0003	256	89	209	7	205	2
13	145	366	0.40	14	0.0497	0.0020	0.2267	0.0090	0.0330	0.0004	189	125	208	7	210	2
14	234	640	0.37	23	0.0537	0.0017	0.2374	0.0073	0.0321	0.0003	361	72	216	6	204	2
15	210	471	0.44	18	0.0527	0.0018	0.2406	0.0087	0.0329	0.0004	317	78	219	7	209	2
16	266	1596	0.17	55	0.0520	0.0012	0.2306	0.0052	0.0320	0.0003	283	55	211	4	203	2
17	230	490	0.47	19	0.0514	0.0018	0.2339	0.0080	0.0330	0.0003	257	84	213	7	209	2
18	208	448	0.46	17	0.0532	0.0020	0.2380	0.0087	0.0324	0.0003	345	83	217	7	206	2
19	257	385	0.67	15	0.0508	0.0020	0.2287	0.0089	0.0327	0.0004	232	58	209	7	207	2
20	186	444	0.42	17	0.0531	0.0019	0.2372	0.0087	0.0323	0.0003	345	81	216	7	205	2

Spot No.	Th (ppm)	U (ppm)	Th/U	Pb (ppm)	Isotopic ratios						Isotopic ages (Ma)					
					$^{207}Pb/^{206}Pb$	±1σ	$^{207}Pb/^{235}U$	±1σ	$^{206}Pb/^{238}U$	±1σ	$^{207}Pb/^{206}Pb$	±1σ	$^{207}Pb/^{235}U$	±1σ	$^{206}Pb/^{238}U$	±1σ
19MY34																
1	11	848	0.01	34	0.0514	0.0013	0.2756	0.0074	0.0388	0.0004	257	59	247	6	245	2
2	104	251	0.42	18	0.0542	0.0020	0.4610	0.0171	0.0619	0.0010	389	81	385	12	387	6
3	502	942	0.53	67	0.0547	0.0012	0.4517	0.0109	0.0595	0.0006	398	53	378	8	372	3
4	20	778	0.03	31	0.0527	0.0014	0.2789	0.0078	0.0382	0.0004	322	63	250	6	242	2
5	12	782	0.02	31	0.0498	0.0016	0.2639	0.0085	0.0382	0.0003	183	74	238	7	242	2
6	105	169	0.62	14	0.0576	0.0027	0.5298	0.0244	0.0671	0.0009	522	106	432	16	419	6
7	407	1196	0.34	78	0.0544	0.0015	0.4233	0.0119	0.0558	0.0006	387	63	358	9	350	4
8	2	203	0.01	8	0.0544	0.0027	0.2892	0.0137	0.0383	0.0005	387	111	258	11	242	3
9	503	989	0.51	103	0.0573	0.0013	0.6847	0.0155	0.0860	0.0011	502	48	530	9	532	6
10	277	738	0.38	56	0.0553	0.0014	0.5034	0.0147	0.0652	0.0009	433	57	414	10	407	5
11	39	454	0.09	21	0.0515	0.0017	0.3051	0.0108	0.0426	0.0006	265	78	270	8	269	4
12	359	1012	0.35	94	0.0544	0.0011	0.5938	0.0119	0.0785	0.0007	387	44	473	8	487	4
13	73	1227	0.06	84	0.0572	0.0013	0.5359	0.0180	0.0671	0.0016	498	45	436	12	419	10
14	16	913	0.02	36	0.0531	0.0010	0.2820	0.0056	0.0384	0.0003	332	44	252	4	243	2
15	181	1185	0.15	48	0.0502	0.0011	0.2734	0.0060	0.0395	0.0004	211	52	245	5	250	2
16	62	450	0.14	18	0.0561	0.0022	0.2965	0.0105	0.0383	0.0004	457	85	264	8	243	2
17	36	415	0.09	17	0.0524	0.0012	0.2810	0.0067	0.0389	0.0004	302	52	251	5	246	2
18	7	660	0.01	26	0.0513	0.0010	0.2742	0.0057	0.0387	0.0004	254	44	246	5	245	3
19	113	766	0.15	32	0.0491	0.0016	0.2686	0.0085	0.0395	0.0003	154	76	242	7	250	2
20	155	635	0.24	28	0.0538	0.0017	0.2945	0.0094	0.0396	0.0004	361	72	262	7	250	2
21	271	427	0.63	20	0.0499	0.0018	0.2685	0.0095	0.0391	0.0004	191	85	241	8	247	2
22	53	338	0.16	14	0.0513	0.0021	0.2777	0.0110	0.0394	0.0004	254	90	249	9	249	3
23	42	1384	0.03	56	0.0512	0.0009	0.2798	0.0067	0.0395	0.0007	256	39	251	5	250	4

Spot No.	**Th (ppm)**	**U (ppm)**	**Th/U**	**Pb (ppm)**	**Isotopic ratios**						**Isotopic ages (Ma)**					
					$^{207}Pb/^{206}Pb$	**±1σ**	**$^{207}Pb/^{235}U$**	**±1σ**	**$^{206}Pb/^{238}U$**	**±1σ**	**$^{207}Pb/^{206}Pb$**	**±1σ**	**$^{207}Pb/^{235}U$**	**±1σ**	**$^{206}Pb/^{238}U$**	**±1σ**
19MY49																
1	118	646	0.18	28	0.0528	0.0016	0.2875	0.0086	0.0395	0.0004	320	66	257	7	250	2
2	255	661	0.39	30	0.0522	0.0016	0.2828	0.0084	0.0392	0.0003	295	64	253	7	248	2
3	261	706	0.37	32	0.0524	0.0015	0.2840	0.0081	0.0392	0.0003	302	65	254	6	248	2
4	284	688	0.41	31	0.0511	0.0017	0.2740	0.0090	0.0389	0.0004	243	78	246	7	246	2
5	228	621	0.37	28	0.0503	0.0016	0.2795	0.0091	0.0402	0.0004	209	40	250	7	254	3
6	246	893	0.28	40	0.0531	0.0014	0.2942	0.0079	0.0401	0.0004	332	29	262	6	254	2
7	165	480	0.34	21	0.0513	0.0017	0.2777	0.0091	0.0392	0.0004	254	76	249	7	248	2
8	81	301	0.27	13	0.0480	0.0022	0.2663	0.0121	0.0401	0.0006	102	104	240	10	254	4
9	146	721	0.20	31	0.0530	0.0015	0.2861	0.0083	0.0391	0.0004	332	65	256	7	247	2
10	139	459	0.30	21	0.0573	0.0020	0.3114	0.0101	0.0396	0.0004	502	71	275	8	250	2
11	55	1099	0.05	51	0.0520	0.0018	0.3103	0.0104	0.0433	0.0005	283	75	274	8	273	3
12	109	488	0.22	21	0.0504	0.0016	0.2764	0.0094	0.0396	0.0004	213	44	248	7	250	2
13	142	430	0.33	23	0.0562	0.0020	0.3779	0.0167	0.0484	0.0012	461	75	325	12	305	7
14	168	620	0.27	27	0.0540	0.0017	0.2964	0.0094	0.0397	0.0004	372	70	264	7	251	2
15	284	916	0.31	41	0.0530	0.0009	0.2889	0.0062	0.0395	0.0006	328	39	258	5	250	3
16	165	597	0.28	27	0.0495	0.0011	0.2699	0.0062	0.0395	0.0004	172	56	243	5	250	3
17	522	1033	0.51	48	0.0518	0.0020	0.2804	0.0118	0.0393	0.0006	276	91	251	9	248	4

Table 2 (*continued*)

Spot No.	Th (ppm)	U (ppm)	Th/U	Pb (ppm)	Isotopic ratios						Isotopic ages (Ma)					
					$^{207}Pb/^{206}Pb$	±1σ	$^{207}Pb/^{235}U$	±1σ	$^{206}Pb/^{238}U$	±1σ	$^{207}Pb/^{206}Pb$	±1σ	$^{207}Pb/^{235}U$	±1σ	$^{206}Pb/^{238}U$	±1σ
18	239	781	0.31	34	0.0502	0.0009	0.2726	0.0060	0.0395	0.0006	211	44	245	5	249	4
19	370	959	0.39	43	0.0520	0.0015	0.2903	0.0104	0.0396	0.0008	287	69	259	8	251	5
20	134	462	0.29	21	0.0504	0.0012	0.2772	0.0066	0.0398	0.0004	217	86	248	5	252	3
21	114	427	0.27	19	0.0520	0.0011	0.2874	0.0059	0.0402	0.0004	283	48	256	5	254	3
22	54	544	0.10	23	0.0517	0.0011	0.2837	0.0062	0.0398	0.0004	272	42	254	5	252	3
23	77	409	0.19	18	0.0495	0.0011	0.2724	0.0066	0.0399	0.0004	172	58	245	5	252	3

0.13 and 0.56. All 20 analyses yielded a weighted mean $^{206}Pb/^{238}U$ age of 211.3 ± 1.1 Ma (Fig. 4B; MSWD = 1.6, 2σ), which is interpreted as the crystallization age of sample 19MY19.

Twenty-two analyses were obtained from 22 zircons in biotite monzogranite sample 19MY20. The zircons show variable abundances of Th (66–473 ppm) and U (298–1564 ppm), with Th/U ratios between 0.1 and 0.55. Twenty analyses yielded a weighted mean $^{206}Pb/^{238}U$ age of 210.4 ± 1.4 Ma (Fig. 4C; MSWD = 2.0, 2σ), which is interpreted as the crystallization age of sample 19MY20. Spots 3 and 4 yielded significantly older $^{206}Pb/^{238}U$ ages of ca. 273 and 394 Ma, respectively, which are interpreted to have been obtained from xenocrysts.

Twenty analyses were obtained from 20 zircons in granodiorite sample 19MY21. The zircons show variable abundances of Th (120–617 ppm) and U (321–2596 ppm), with Th/U ratios between 0.15 and 0.67. All 20 analyses yielded a weighted mean $^{206}Pb/^{238}U$ age of 206.7 ± 1.1 Ma (Fig. 4C; MSWD = 1.4, 2σ), which is interpreted as the crystallization age of sample 19MY21.

For the granodiorite (Sample 19MY34), 23 analyses were obtained from 23 zircons. The zircons show variable abundances of Th (2–503 ppm) and U (169–1384 ppm), with Th/U ratios between 0.01 and 0.63. A weighted mean $^{206}Pb/^{238}U$ age of 245.6 ± 1.9 Ma (Fig. 4C; MSWD = 1.9, 2σ) was calculated from 14 grains and is interpreted as the crystallization age of sample 19MD34. Spots 2, 3, 6, 7, 9, 10, 11, 12, and 13 yielded significantly older $^{206}Pb/^{238}U$ ages of ca. 387, 372, 419, 350, 532, 407, 269, 487, and 419 Ma, respectively. As such, those grains are interpreted to be xenocrysts.

Twenty-three analyses were obtained from 23 zircons in granodiorite sample 19MY49. The zircons show variable abundances of Th (54–522 ppm) and U (301–1099 ppm), with Th/U ratios ranging between 0.1 and 0.51. Twenty-one analyses yielded a weighted mean $^{206}Pb/^{238}U$ age of 250.2 ± 1.1 Ma (Fig. 4C; MSWD = 0.88, 2σ), which is interpreted as the crystallization age of sample 19MY49. Spots 11 and 13 yielded significantly older $^{206}Pb/^{238}U$ ages of ca. 273 and 305 Ma, respectively, which are interpreted to have been obtained from xenocrysts.

Overall, our zircon U–Pb dating results indicate that the Kyaing Tong granites were emplaced around 207–216 Ma, whereas the Tachileik granites were emplaced around 246–250 Ma.

4.2. Major and trace elements composition

The results of geochemical analyses are shown in Table 3. Harker diagrams (Fig. 5) show that many of the Kyaing Tong and Tachileik granitoids exhibit much geochemical similarity. In general, as the silica contents increase in the granitoids, TiO_2, Al_2O_3, FeO^{tot}, MgO, CaO, and MnO contents decrease, while K_2O is the only component to show a positive correlation with SiO_2. A poor correlation is observed between silica and Na_2O. All samples plot in the peraluminous field on a A/NK versus A/CNK diagram, except for samples 19MD26 and 19MD27 (Fig. 6A), which are metaluminous granites. Here, A/NK and A/CNK are defined as the molar ratios of $Al_2O_3/(Na_2O + K_2O)$ and $Al_2O_3/(CaO + Na_2O + K_2O)$, respectively. Hence, a A/CNK plot cannot be used to effectively discriminate the Kyaing Tong and Tachileik granites.

Chondrite-normalized REE patterns and primitive mantle-normalized trace element spidergrams are shown in Fig. 7. All chondrite-normalized REE patterns for the Kyaing Tong granites show light REE enrichments, with $(La/Yb)_N$ ratios of 6.5 to 22.1 and negative Eu anomalies (δEu = 0.5–0.9). They have a range of total REE ($\sum$REE) concentrations between 92 and 399 ppm. Similarly, chondrite-normalized REE patterns for the Tachileik granites also show light REE enrichments, with $(La/Yb)_N$ ratios of 3.5 to 12.9 and negative Eu anomalies (δEu = 0.6–0.9). They have a range of $\sum$REE concentrations between 90 and 195 ppm (Fig. 7A). Spidergrams show similarities between the Kyaing Tong granites and Tachileik granites, with characteristic negative anomalies in Ba, Nb, Ta, Sr, and Ti, and a positive anomaly in Pb (Fig. 7B). The REE and trace element patterns in these granites resemble those of schist from the Lancang Group (Fig. 7C and D). The most significant geochemical differences occur between these granites and amphibolite of the Lancang Group, southeastern Tibetan Plateau (*Peng* et al., 2020), particularly in terms of light REE, Eu, Th, U, K, and Sr (Fig. 7C and D). Zircon saturation thermometry (*Boehnke* et al., 2013) was applied to estimate the temperatures of the granitic melts. The Kyaing Tong and Tachileik granites exhibit similar temperatures of T_{Zr} = 655–791 °C and T_{Zr} = 685–802 °C, respectively.

Enrichment of high field strength elements, such as Zr, Nb, and Ce, is evident in the plots of *Whalen* et al. (1987) (Fig. 6C), in which it appears that some of the Kyaing Tong granitoids (samples 19MD26 and 19MD27) fall into the A-type field. The high Rb contents (166–354 ppm) are observed in the Kyaing Tong granites, while Tachileik granites have low Rb contents (105–148 ppm).

4.3. Sr–Nd isotope data

The results of Sr–Nd isotopic analyses are shown in Table 4. The Kyaing Tong granites have high and variable initial $^{87}Sr/^{86}Sr$ ratios (0.717735–0.731271) and low $^{143}Nd/^{144}Nd$ ratios (0.511806–0.511988). The ε_{Nd} (t = 215 Ma) values mainly range from −14.2 to −10.4, corresponding to T_{DM2} (two-stage model ages) ages of 1835–2143 Ma. The Sr–Nd isotopic data of the Kyaing Tong granites resemble those of the Tachileik granites, which have high initial $^{87}Sr/^{86}Sr$ ratios (0.715336–0.722712) and negative ε_{Nd} (t = 250 Ma) values (−12.4 to −11.3). In Fig. 8, the Kyaing Tong and Tachileik granites plot in the field of Main Range Province and Lincang granites; however, they are different from the Eastern Province granites in Malaysia. Fig. 8 further shows that these granites may be generated by mixing of two end-member lithologies: amphibolite and schist.

5. Discussion

5.1. Genetic type: I-type or S-type?

The geochemical and isotopic characteristics of granites have previously been interpreted using the I- and S-type classification scheme of *Chappell and White* (1974). In that study, granites formed by igneous-sourced melt were described as I-type, whereas those formed from sedimentary-sourced melt were called S-type. The Southeast Asian tin

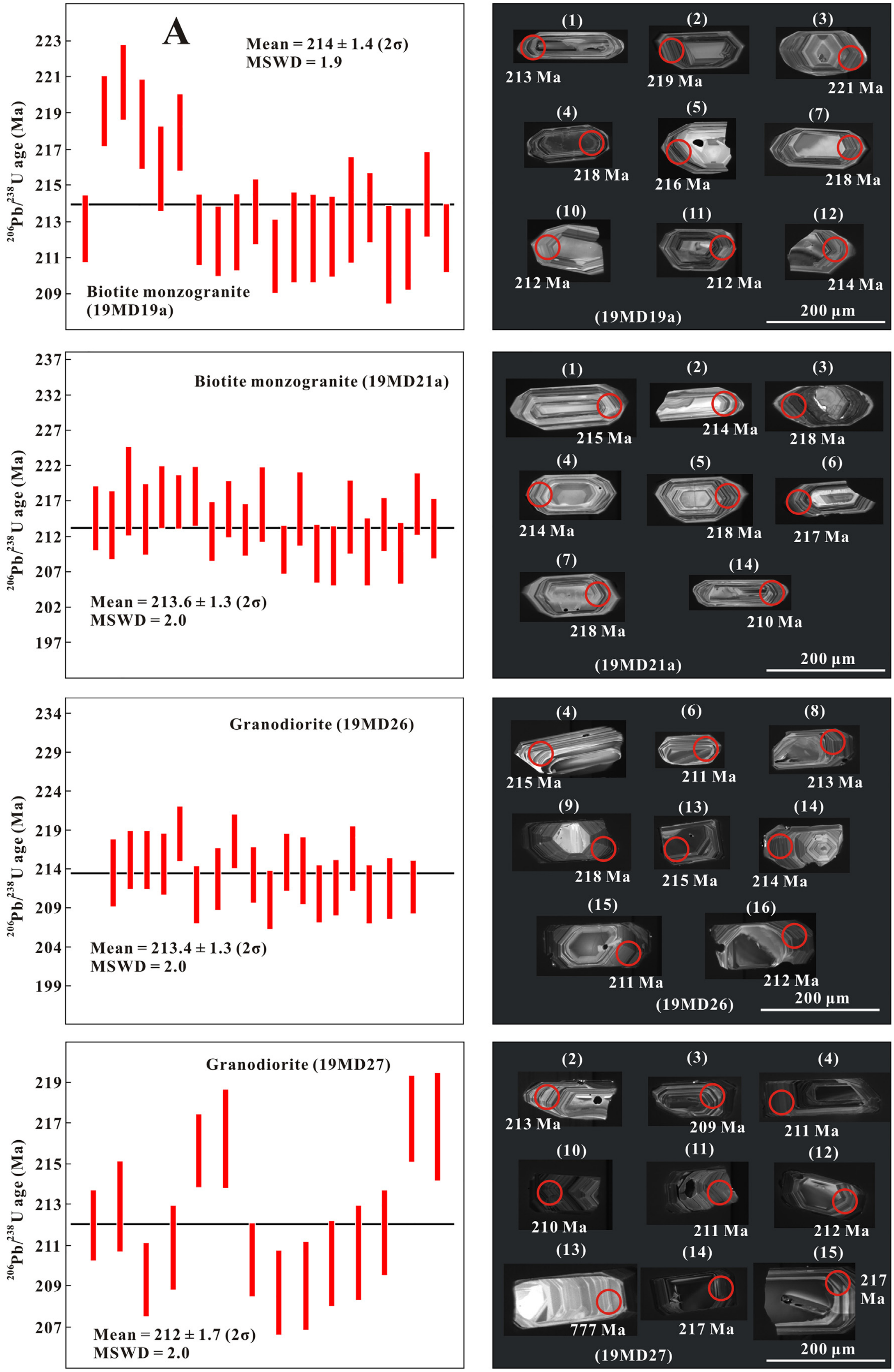
A
Mean = 214 ± 1.4 (2σ)
MSWD = 1.9
Biotite monzogranite
(19MD19a)
206Pb/238U age (Ma)
223
221
219
217
215
213
211
209
(1)
213 Ma
(2)
219 Ma
(3)
221 Ma
(4)
218 Ma
(5)
216 Ma
(7)
218 Ma
(10)
212 Ma
(11)
212 Ma
(12)
214 Ma
(19MD19a)
200 μm
Biotite monzogranite (19MD21a)
Mean = 213.6 ± 1.3 (2σ)
MSWD = 2.0
206Pb/238U age (Ma)
237
232
227
222
217
212
207
202
197
(1)
215 Ma
(2)
214 Ma
(3)
218 Ma
(4)
214 Ma
(5)
218 Ma
(6)
217 Ma
(7)
218 Ma
(14)
210 Ma
(19MD21a)
200 μm
Granodiorite (19MD26)
Mean = 213.4 ± 1.3 (2σ)
MSWD = 2.0
206Pb/238U age (Ma)
234
229
224
219
214
209
204
199
(4)
215 Ma
(6)
211 Ma
(8)
213 Ma
(9)
218 Ma
(13)
215 Ma
(14)
214 Ma
(15)
211 Ma
(16)
212 Ma
(19MD26)
200 μm
Granodiorite (19MD27)
Mean = 212 ± 1.7 (2σ)
MSWD = 2.0
206Pb/238U age (Ma)
219
217
215
213
211
209
207
(2)
213 Ma
(3)
209 Ma
(4)
211 Ma
(10)
210 Ma
(11)
211 Ma
(12)
212 Ma
(13)
777 Ma
(14)
217 Ma
(15)
217 Ma
(19MD27)
200 μm

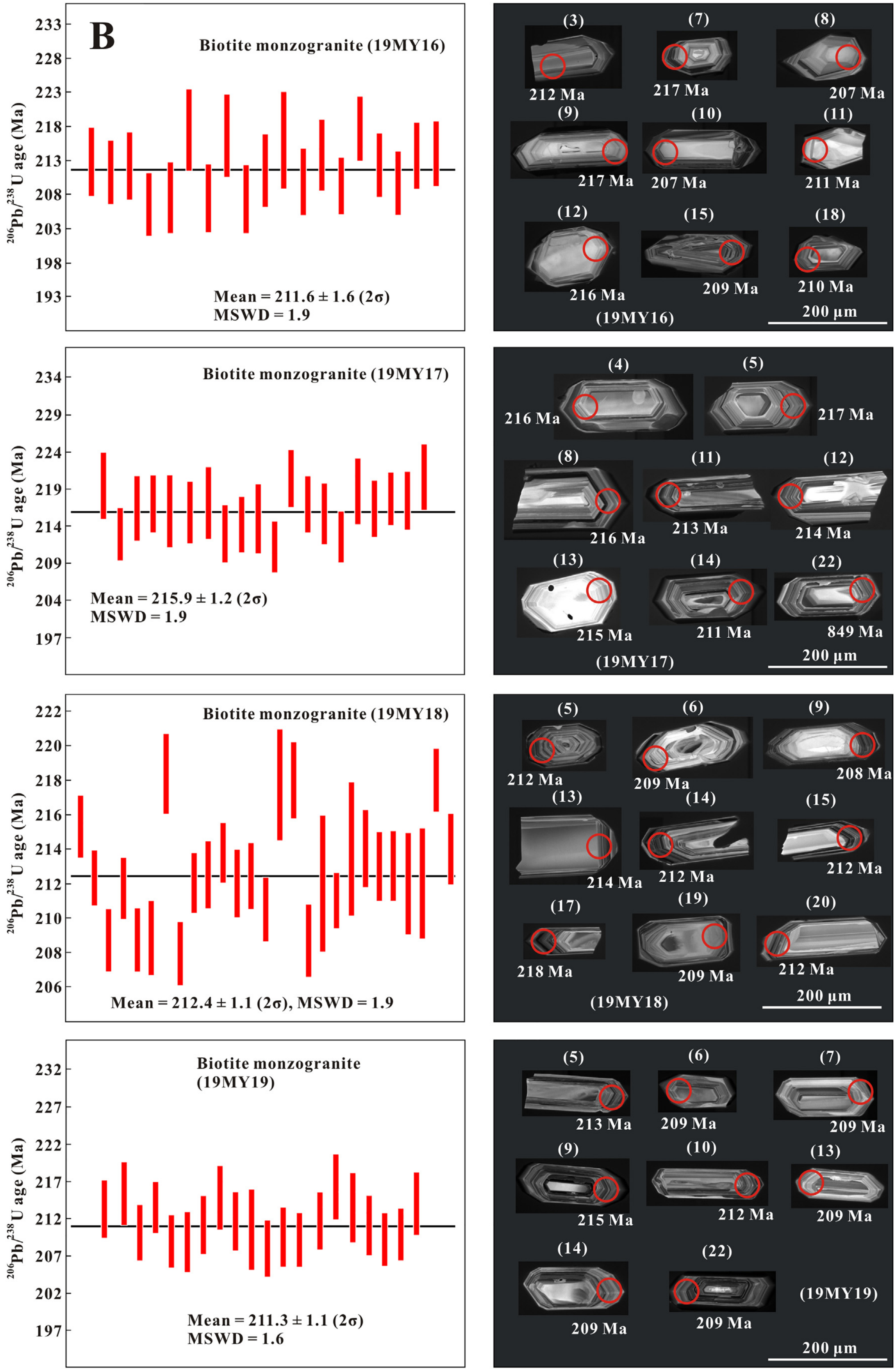
B
Biotite monzogranite (19MY16)
206Pb/238U age (Ma)
Mean = 211.6 ± 1.6 (2σ)
MSWD = 1.9
(3) 212 Ma
(7) 217 Ma
(8) 207 Ma
(9) 217 Ma
(10) 207 Ma
(11) 211 Ma
(12) 216 Ma
(15) 209 Ma
(18) 210 Ma
(19MY16)
200 μm
Biotite monzogranite (19MY17)
Mean = 215.9 ± 1.2 (2σ)
MSWD = 1.9
(4) 216 Ma
(5) 217 Ma
(8) 216 Ma
(11) 213 Ma
(12) 214 Ma
(13) 215 Ma
(14) 211 Ma
(22) 849 Ma
(19MY17)
200 μm
Biotite monzogranite (19MY18)
Mean = 212.4 ± 1.1 (2σ), MSWD = 1.9
(5) 212 Ma
(6) 209 Ma
(9) 208 Ma
(13) 214 Ma
(14) 212 Ma
(15) 212 Ma
(17) 218 Ma
(19) 209 Ma
(20) 212 Ma
(19MY18)
200 μm
Biotite monzogranite
(19MY19)
Mean = 211.3 ± 1.1 (2σ)
MSWD = 1.6
(5) 213 Ma
(6) 209 Ma
(7) 209 Ma
(9) 215 Ma
(10) 212 Ma
(13) 209 Ma
(14) 209 Ma
(22) 209 Ma
(19MY19)
200 μm

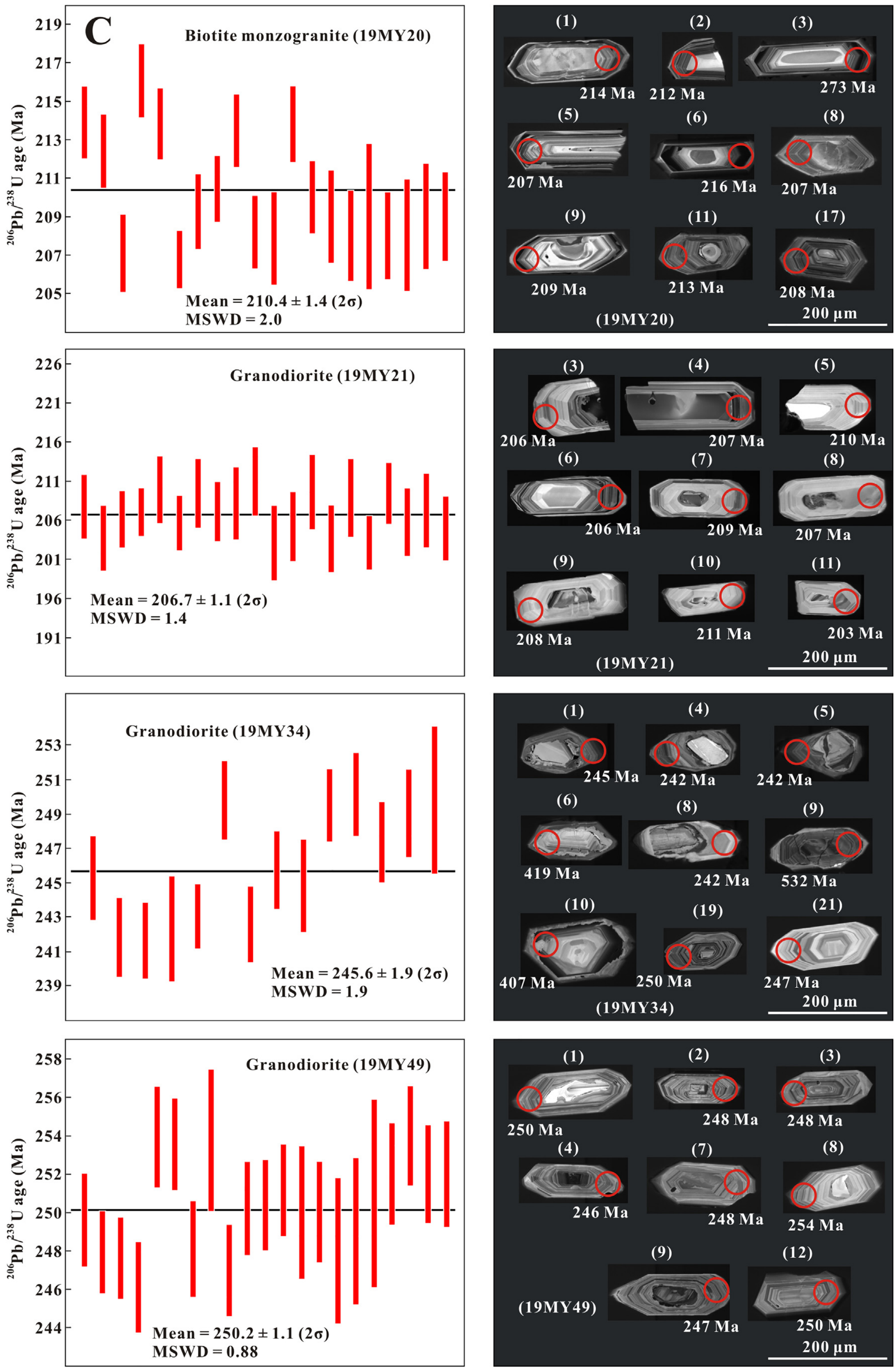

Fig. 4. U–Pb isotopic analyses of zircons in the Kyaing Tong and Tachileik granites from eastern Myanmar, showing representative CL and $^{206}Pb/^{238}U$ ages of analyzed zircons. Red circle: analytical spot of U–Pb isotope. The results indicate that the Kyaing Tong and Tachileik granites were formed at 207–216 Ma and 246–250 Ma, respectively.

Table 3
Contents of major (wt%) and trace elements (ppm) for Kyaing Tong and Tachileik granites.

Sample	19MD19a	19MD20a	19MY16	19MY19	19MD21a	19MY17	19MY18	19MY20
	Biotite monzogranite							
SiO_2	70.20	70.11	70.57	68.91	65.25	67.51	67.67	68.23
Al_2O_3	13.80	13.75	13.91	13.33	14.42	14.21	14.72	14.44
FeO^{tot}	4.07	2.14	3.91	4.58	5.31	4.60	3.93	3.77
CaO	1.53	1.35	1.41	1.96	2.78	2.35	2.30	2.16
MgO	1.89	0.95	1.78	2.59	3.05	2.49	2.27	2.16
K_2O	3.82	6.42	3.73	4.05	3.33	3.79	4.46	4.49
Na_2O	2.25	2.11	2.28	2.04	2.24	2.39	2.43	2.39
TiO_2	0.60	0.29	0.54	0.70	0.78	0.67	0.60	0.55
P_2O_5	0.17	0.21	0.07	0.25	0.26	0.26	0.33	0.27
MnO	0.05	0.04	0.06	0.05	0.07	0.05	0.04	0.04
LOI	0.96	1.98	1.07	0.94	1.62	0.87	0.75	0.74
Total	99.33	99.36	99.32	99.38	99.11	99.18	99.50	99.24
Li	22.5	16.2	33.6	22.1	23.4	21.4	20.1	17.6
Be	2.59	1.39	5.55	2.14	2.27	1.33	1.88	1.68
Sc	11.6	9.56	12.2	13.4	15.2	14.0	12.2	11.0
V	79.1	35.4	71.8	66.4	86.9	75.1	66.9	58.4
Cr	65.5	31.8	63.2	108	105	90.9	70.8	61.6
Co	10.6	6.07	11.4	13.4	13.2	13.1	11.0	10.1
Ni	27.2	14.3	27.4	42.9	30.1	31.7	32.6	28.0
Cu	18.2	7.83	19.3	15.9	17.2	14.0	10.9	10.3
Zn	57.3	27.5	52.9	66.0	88.1	82.4	60.4	53.4
Ga	19.0	13.8	17.9	19.4	20.8	20.6	19.6	18.9
Rb	210	258	186	218	193	218	211	203
Sr	124	118	114	137	180	148	163	165
Y	30.8	19.3	49.5	28.9	31.5	29.3	35.2	32.8
Zr	163	88.5	162	166	132	193	194	182
Nb	17.7	10.2	13.3	18.7	17.8	20.9	16.7	15.4
Mo	1.98	0.696	0.865	0.862	1.58	0.941	0.894	0.811
In	0.076	0.060	0.073	0.086	0.077	0.085	0.072	0.069
Cs	9.63	4.52	19.0	9.74	9.47	9.20	6.93	7.23
Ba	745	617	639	974	532	826	1196	1256
La	50.3	18.1	43.2	34.3	45.8	33.6	35.5	40.4
Ce	96.5	36.7	83.8	69.7	90.2	70.0	72.0	77.8
Pr	10.2	4.15	9.00	7.64	10.5	7.56	8.00	8.54
Nd	40.4	16.1	34.0	29.0	37.9	28.8	30.3	31.2
Sm	8.04	3.64	6.85	5.99	7.67	5.99	6.66	6.59
Eu	1.21	1.04	1.15	1.20	1.33	1.38	1.43	1.42
Gd	6.90	3.38	6.44	5.39	6.40	5.53	6.07	5.76
Tb	1.01	0.562	1.05	0.852	1.01	0.856	0.993	0.930
Dy	5.77	3.48	7.30	5.36	5.80	5.36	6.54	5.84
Ho	1.08	0.687	1.67	1.06	1.13	1.10	1.31	1.21
Er	2.84	1.86	4.75	2.83	3.11	2.91	3.41	3.22
Tm	0.405	0.278	0.715	0.419	0.448	0.413	0.499	0.456
Yb	2.58	1.85	4.74	2.78	3.10	2.67	3.20	2.97
Lu	0.379	0.275	0.721	0.402	0.464	0.396	0.463	0.426
Hf	4.58	2.50	4.78	4.49	3.80	5.35	5.50	5.24
Ta	1.92	1.24	1.61	1.76	1.90	1.85	1.58	1.47
W	2.57	2.37	2.37	2.56	2.10	2.02	2.03	1.67
Pb	31.5	53.0	37.1	35.0	36.6	35.4	44.6	46.9
Bi	0.422	0.358	0.725	0.391	0.358	0.419	0.335	0.358
Th	23.9	10.0	20.6	17.2	20.7	15.1	16.8	19.0
U	5.28	9.34	8.99	5.99	4.79	5.54	5.43	4.82
$(La/Yb)_N$	14.0	7.0	6.5	8.9	10.6	9.0	8.0	9.8
δEu	0.5	0.9	0.5	0.6	0.6	0.7	0.7	0.7
∑REE	228	92	205	167	215	167	176	187
T_{Zr} (°C)	773	684	778	758	725	767	763	759

Sample	19MD26	19MD27	19MY21	19MY35	19MY36	19MY34	19MY37	19MY49	PM07-7-b1
	Granodiorite			Biotite monzogranite		Granodiorite			two-mica quartz schist
SiO_2	66.66	66.92	63.47	70.17	73.46	67.58	72.89	67.03	76.21
Al_2O_3	14.43	14.05	14.32	14.84	13.25	14.10	13.67	14.77	10.72
FeO^{tot}	3.82	3.83	5.80	3.12	1.68	5.47	2.17	4.89	4.03
CaO	2.76	2.87	3.84	1.57	1.19	1.25	0.98	3.45	0.82
MgO	2.31	2.39	3.23	1.52	0.78	2.70	1.03	2.23	1.68
K_2O	5.67	5.07	3.14	3.87	4.75	3.21	4.24	3.02	2.62
Na_2O	2.09	2.16	2.02	1.64	2.18	0.89	2.18	1.95	1.31
TiO_2	0.57	0.55	0.78	0.37	0.22	0.64	0.25	0.53	0.52
P_2O_5	0.30	0.29	0.25	0.22	0.11	0.23	0.11	0.11	0.15
MnO	0.07	0.08	0.09	0.05	0.04	0.07	0.04	0.08	0.05
LOI	0.73	1.32	1.95	2.00	1.72	3.44	1.92	1.07	1.56
Total	99.40	99.53	98.89	99.38	99.38	99.57	99.48	99.13	99.67
Li	28.1	48.0	58.8	11.7	6.98	18.6	9.62	33.3	81.1

(continued on next page)

Table 3 (*continued*)

Sample	19MD26	19MD27	19MY21	19MY35	19MY36	19MY34	19MY37	19MY49	PM07-7-b1
Be	11.0	12.0	4.23	1.81	0.886	2.47	1.23	2.29	4.97
Sc	12.0	12.8	16.2	10.2	8.67	12.7	8.31	14.3	12.9
V	69.2	66.6	123	53.8	31.3	123	35.7	97.2	59.6
Cr	86.6	85.3	123	41.5	23.2	96.3	26.6	52.3	58.4
Co	9.46	9.93	16.5	7.95	4.84	15.4	5.17	12.8	7.53
Ni	20.1	20.5	36.0	20.2	12.5	53.8	13.6	24.5	16.4
Cu	12.6	10.4	24.7	31.4	11.6	76.7	14.3	35.6	17.7
Zn	65.2	64.7	68.8	63.4	47.2	90.7	57.3	66.4	124
Ga	19.4	19.3	19.8	16.7	13.6	17.7	14.6	17.4	15.7
Rb	354	330	166	105	144	148	132	136	258
Sr	407	358	255	131	123	64.6	95.9	134	61.4
Y	36.6	34.7	34.7	36.1	31.3	28.3	32.5	32.0	25.5
Zr	326	287	75.9	108	68.3	136	89.6	122	119
Nb	28.7	27.7	18.7	10.1	8.98	12.6	10.2	9.99	12.2
Mo	2.00	1.58	2.22	0.499	0.656	1.45	0.626	0.419	2.92
In	0.081	0.125	0.071	0.050	0.061	0.064	0.069	0.063	0.0753
Cs	23.3	26.5	7.40	2.36	3.97	4.48	4.49	6.77	38
Ba	1634	1276	868	979	502	634	465	470	469
La	91.9	84.3	68.2	27.2	17.8	43.2	19.4	34.6	48.2
Ce	172	168	131	55.5	33.0	82.1	37.2	70.3	99.7
Pr	20.1	19.2	13.8	5.86	3.85	8.73	4.3	7.41	10.3
Nd	73.0	69.9	54.1	23.2	14.4	34.3	16.6	28.6	38.3
Sm	13.9	12.9	10.0	4.92	3.23	6.72	3.63	6.03	7.28
Eu	2.13	1.82	1.72	1.47	0.909	1.25	0.923	1.09	1.18
Gd	9.46	9.16	8.04	4.83	3.24	5.96	3.56	5.46	6.07
Tb	1.34	1.28	1.18	0.852	0.624	0.935	0.675	0.848	0.927
Dy	6.56	6.38	6.45	5.82	4.61	5.41	4.77	5.34	5.08
Ho	1.22	1.17	1.22	1.24	1.00	1.02	1.06	1.12	0.904
Er	3.35	3.26	3.33	3.48	3.03	2.68	3.19	3.16	2.32
Tm	0.442	0.422	0.447	0.552	0.529	0.372	0.546	0.471	0.304
Yb	2.98	2.91	2.78	3.71	3.69	2.41	3.72	3.09	2
Lu	0.442	0.434	0.391	0.551	0.556	0.351	0.572	0.494	0.288
Hf	9.47	8.78	2.19	3.07	2.12	3.76	2.74	3.57	3.3
Ta	3.33	3.10	1.39	1.17	1.27	1.05	1.33	0.98	1.28
W	5.10	5.50	1.92	1.42	2.04	1.38	1.37	1.41	1.94
Pb	89.6	69.2	30.0	49.6	57.1	29.9	56.2	30.4	29
Bi	0.668	0.521	0.267	1.24	0.486	0.199	0.562	0.36	3.36
Th	73.3	66.5	37.4	10.7	7.48	16.2	7.90	15.4	20.4
U	22.5	19.0	6.93	6.34	8.18	3.30	6.10	3.22	4.5
$(La/Yb)_N$	22.1	20.8	17.6	5.26	3.5	12.9	3.7	8.0	17.3
δEu	0.6	0.5	0.6	0.9	0.9	0.6	0.8	0.6	0.5
∑REE	399	381	303	139	90	195	100	168	223
T_{Zr} (°C)	791	779	655	751	685	802	724	720	

Note: LOI = loss on ignition. $\delta Eu = Eu_N/(Sm_N \times Gd_N)^{0.5}$, N stands for chondrite-normalized (*Sun and McDonough,* 1989). T_{Zr} (°C) is defined as 10,108/{lnD + 1.48 + [1.16(M - 1)]} (*Boehnke* et al., 2013), M is defined as the cation ratio (Na + K + 2Ca)/(Al × Si), where D is the concentration ratio of Zr in zircon (496,000 ppm) to that in the sample (*Watson and Harrison,* 1983).

belt has traditionally been divided into a Permian to Early Triassic Eastern Province dominated by arc-related I-type granitoids and a Late Triassic Main Range Province dominated by collision-related S-type granitoids, which are separated by Paleo-Tethys sutures (*Cobbing* et al., 1986; *Hutchison,* 1977; *Mitchell,* 1977). However, *Ng* et al. (2015a) argued that direct application of the I- and S-type classification scheme cannot account for many of the characteristics exhibited by Malaysian granitoids. Instead, *Searle* et al. (2012), *Ghani* et al. (2013), and *Ng* et al. (2015a) suggest that the Malaysian granitoids can be divided by the Bentong-Raub suture zone into an I-type Eastern Province and a transitional I/S-type Main Range Province.

Mineralogically, Kyaing Tong granite samples 19MD26, 19MD27, and 19MY21 contain diagnostic I-type minerals, such as hornblende (Fig. 3E, Table 1) and sphene (Table 1). The presence of hornblende in samples 19MD26 and 19MD27 is consistent with their metaluminous geochemistry (Fig. 6A); however, the Tachileik pluton is dominated by hornblende-free and biotite-bearing monzogranite and granodiorite. The mineralogical characteristics of these hornblende-free granites resemble those of the roof zones of the Eastern Province I-type granites in Malaysia (*Ng* et al., 2015a). Therefore, we consider that both the Kyaing Tong and Tachileik granites are of I-type affinity.

5.2. Origin of granites

The two most widely accepted processes for the generation of silicic magma are partial melting of pre-existing crustal rocks (*Dufek and Bergantz,* 2005; *Sisson* et al., 2005) and differentiation by crystallization of mantle-derived magmas (*Mortazavi and Sparks,* 2004; *Pichavant* et al., 2002). The Kyaing Tong and Tachileik granites are characterized by low FeO^{tot}/MgO ratios of 1.6–2.3 (Fig. 6C) and nearly chondritic Zr/Hf ratios of 32.2–37. Therefore, these unfractionated geochemical features rule out the possibility of differentiation and crystallization of mantle-derived magmas. If partial melting is considered as the mechanism of formation, possible source rocks for the Kyaing Tong and Tachileik granites can be determined by comparing their measured Sr–Nd isotopic compositions with those of surrounding basement rocks. The Lancang Group consists mainly of amphibolite, schist and gneiss of amphibolite-facies that represent the lower continental crust of the Indochina block (*Zhong,* 1998). In this study, the Sr–Nd isotopic compositions of the granitoids are compared with isotope data obtained from amphibolite and schist from the Lancang Group. Amphibolite sample D6142H7 (initial $^{87}Sr/^{86}Sr = 0.705$, ε_{Nd} (250 Ma) = +1.3, *Peng* et al., 2020) and two-mica quartz schist sample PM07-7-b1 in this

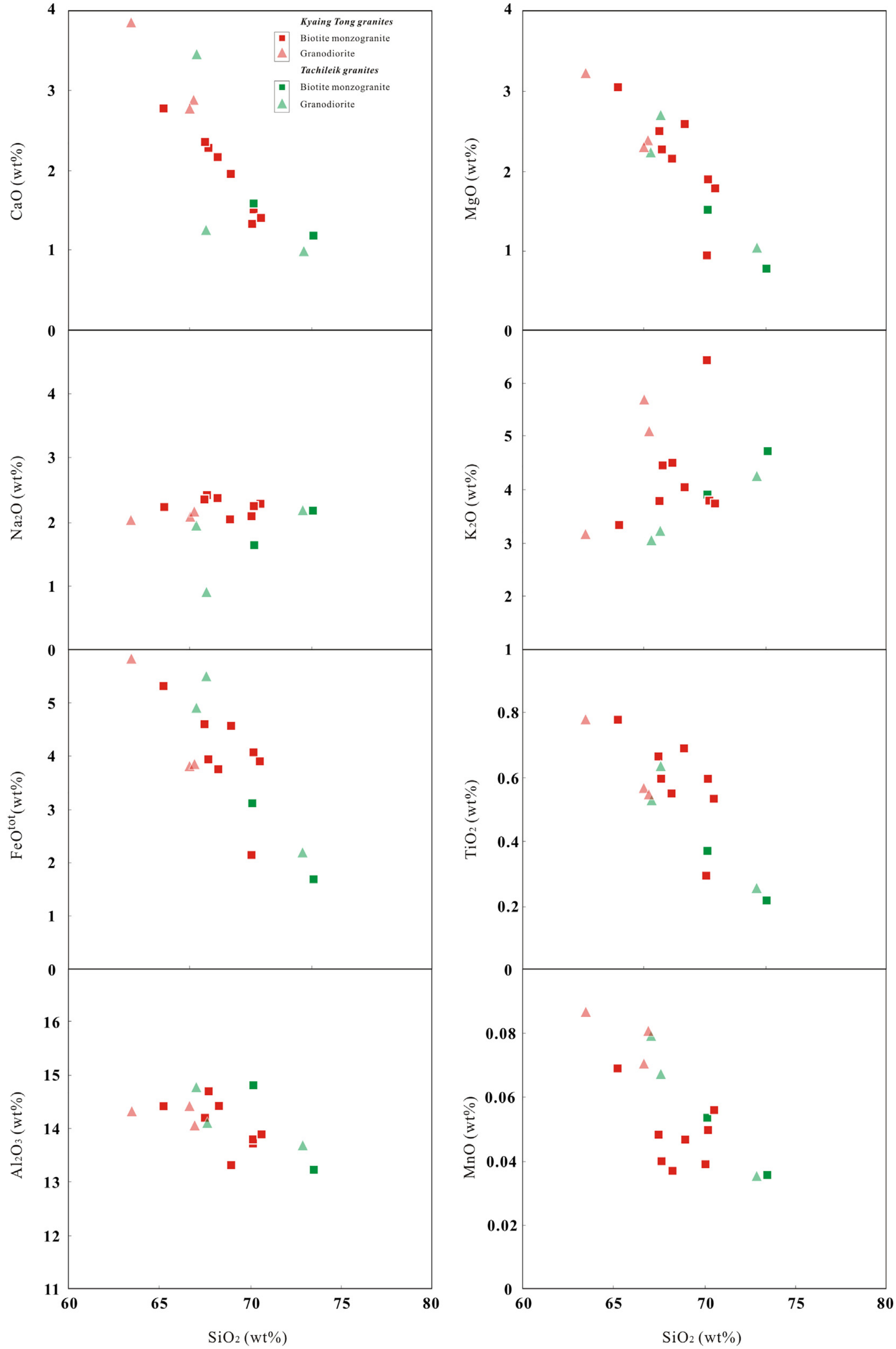

Fig. 5. Harker diagrams for the Kyaing Tong and Tachileik granites. As the silica contents increase in the granitoids, TiO_2, Al_2O_3, FeO^{tot}, MgO, CaO, and MnO decrease, while K_2O is alone in showing a positive correlation with silica.

study (initial $^{87}Sr/^{86}Sr$ = 0.737, ε_{Nd} (250 Ma) = −16.2) of the Lancang Group were selected as end-members in Fig. 8. Our results suggest that mixing of both components can generate these granitoids (Fig. 8). The Sr–Nd isotopic data of amphibolites from the Lancang Group resemble those of the Eastern Province granites, which have low initial $^{87}Sr/^{86}Sr$ ratios (0.6976–0.7074) and weakly

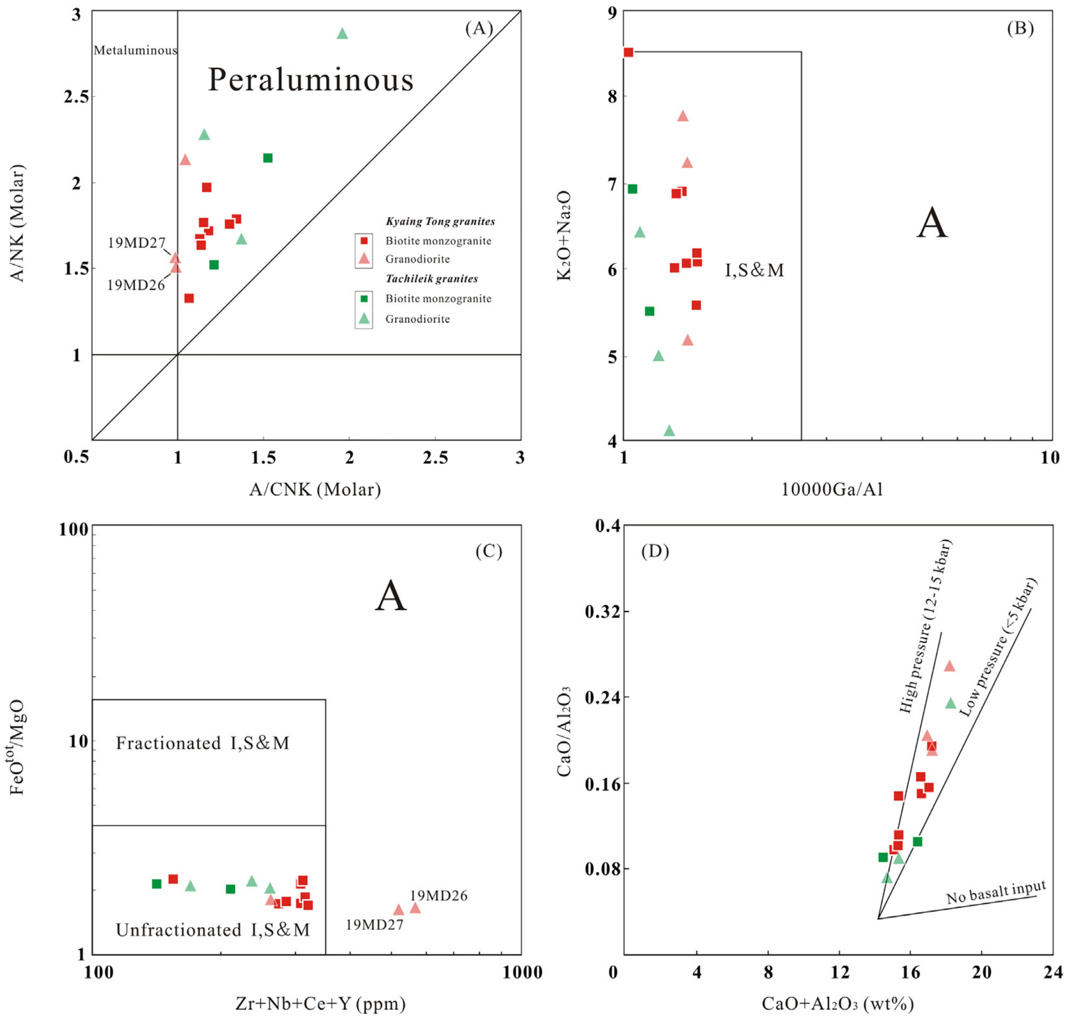

Fig. 6. (A) A/NK vs. A/CNK plot showing the peraluminous nature of the Kyaing Tong and Tachileik granites. A = Al_2O_3, N = Na_2O, K = K_2O, C = CaO (all in molar proportion). (B) ($K_2O + Na_2O$) vs. 10000Ga/Al classification and (C) FeO^{tot}/MgO vs. (Zr + Nb + Ce + Y) classification diagrams (*Whalen* et al., 1987), indicating that most of the Kyaing Tong and Tachileik granites are unfractionated I-, S- and M-types. However, two Kyaing Tong granites have A-type geochemical characteristics. FG: Fractionated felsic granites; OGT: unfractionated M-, I- and S-type granites. (D) CaO + Al_2O_3 vs. CaO/Al_2O_3 diagram (after *Patiño*, 1999) of the Kyaing Tong and Tachileik granites. Lines indicating trends are high-pressure, low-pressure, and magmas with no basalt input, respectively.

negative ε_{Nd} (t) values (−5.3 to +0.6) (*Ng* et al., 2015a). Therefore, *Ng* et al. (2015a) suggested that partial melting of amphibolites of the Kontum massif could have formed the parental magma of the Eastern Province granites. We suggest that incorporation of schist played a minimal role in forming the Eastern Province granites, but was much more important for forming the Main Range Province parental magma. Our Sr–Nd isotopic data from this latter region suggest that up to 40–60% and 50–80% of schist was incorporated into the parental magma of the Tachileik and Kyaing Tong pluton, respectively. High Rb contents (166–354 ppm) of the Kyaing Tong granites are consistent with the observation of more evolved source material in their parental magma. Therefore, we consider that the Tachileik and Kyaing Tong plutons were derived from partial melting of the amphibolite and underwent assimilation of two-mica quartz schist.

Support for this interpretation comes from numerous experimental studies of partially melted amphibolitic materials at high pressure generating tonalitic–andesitic–rhyolitic melt. In response to basaltic thermal input to the lower continental crust at pressures greater than 10 kbar, dehydration melting of amphibole can form tonalitic melt, garnet, and clinopyroxene (*Wolf and Wyllie*, 1994). The experiments of *Sisson* et al. (2005) demonstrated that small amounts of partial melting (0.1–0.3 melt fraction) of a mafic source rock at 8 kbar can produce high-potassium dacitic to rhyolitic melts; however, low melt fractions produced via dehydration melting of amphibolite, as predicted by thermal modeling, typically produces moderate to mildly peraluminous melts. As the melt fraction increases, the aluminum content decreases, and the melts become meta-aluminous as they approach the amphibole-out boundary (*Rapp and Watson*, 1995). On a CaO + Al_2O_3 versus CaO/Al_2O_3 diagram (Fig. 6D), the Kyaing Tong and Tachileik granites lie on high-pressure trends, which are consistent with this experimental result that partial melting of amphibolite at high pressures forms granitic melt. Furthermore, the genetic relationship between granitic melt and amphibolite residuum predicted by dehydration experiments at lower pressures in the crust is expressed in the geological record of the Lancang Group, which is also regarded as a viable analogue of the lower continental crust of Indochina (*Zhong*, 1998).

Amphibolite within the Lancang Group has been interpreted as metamorphosed basalt and formed during the Silurian (U–Pb zircon age of 434–437 Ma; *Peng* et al., 2020), which is similar to zircon U–Pb ages produced by gneisses within the Kontum massif (*Carter* et al., 2001). The amphibolites are dominated by hornblende and plagioclase, contain minor clinopyroxene and garnet with a cumulate texture, and were intruded by Triassic granites (*Peng* et al., 2020). In such cases, hornblende, plagioclase, clinopyroxene, and garnet are expected to be part of the residue of a melt-depleted source region. Therefore, the trace element concentration of granitic melts formed in this geological

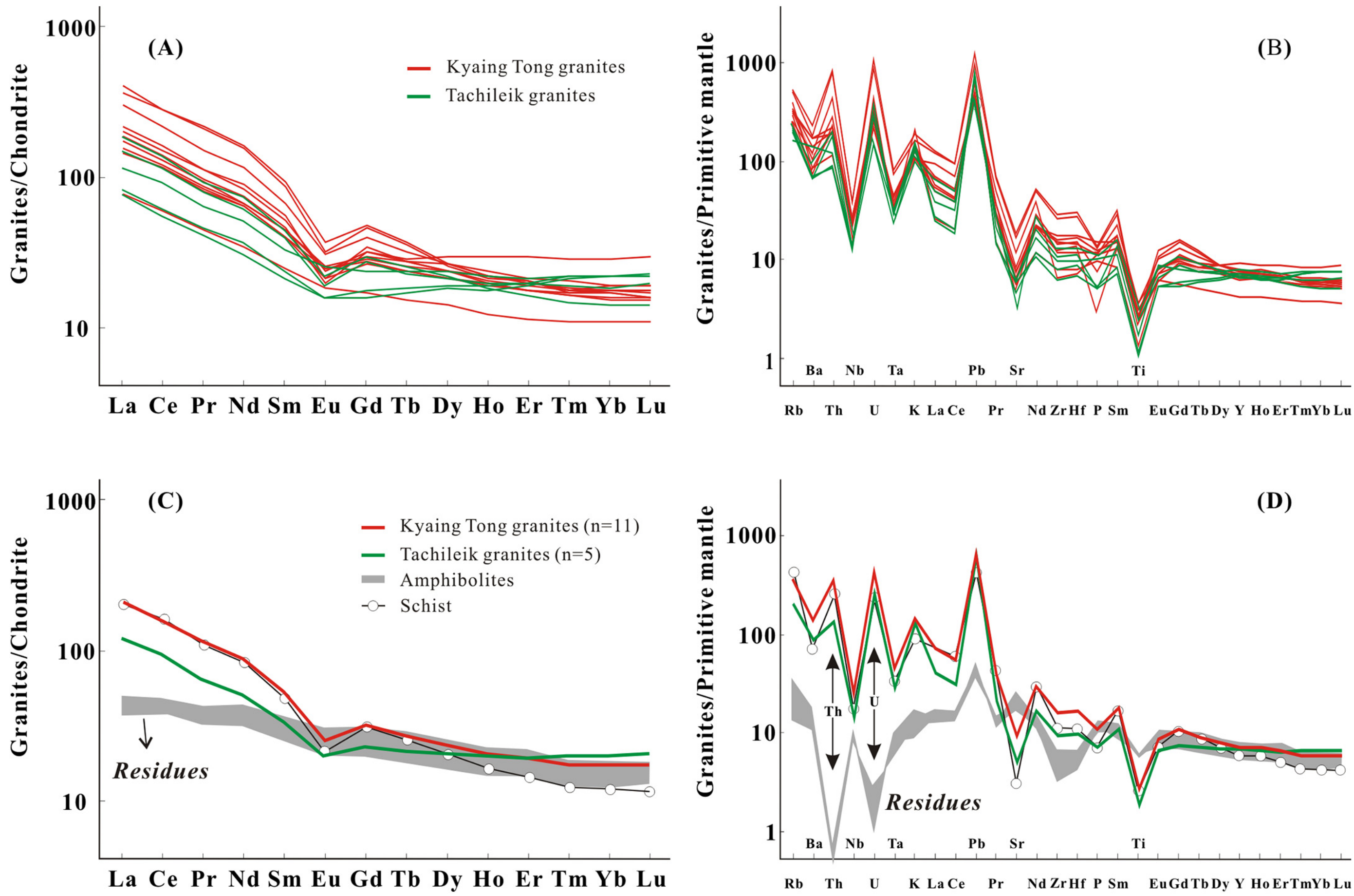

Fig. 7. Chondrite-normalized REE and Primitive mantle-normalized trace element patterns of the Kyaing Tong and Tachileik granites. Chondrite and Primitive mantle values are from Sun and McDonough (1989). Compositions of amphibolite and two-mica quartz schist of the Lancang Group are from Peng et al. (2020) and this study (Table 3), respectively.

Table 4
Sr–Nd isotopic compositions of Kyaing Tong and Tachileik granites in eastern Myanmar.

Sample no.	Location	Rb	Sr	^{87}Rb/^{86}Sr	^{87}Sr/^{86}Sr	2σ	(^{87}Sr/^{86}Sr)$_i$	Sm	Nd	^{147}Sm/^{144}Nd	^{143}Nd/^{144}Nd	2σ	ε_{Nd} (0)	ε_{Nd} (t)	T_{DM} (Ma)	T_{DM2} (Ma)	$f_{Sm/Nd}$
19MD19a	Kyaing Tong	210	124	4.9185	0.746322	0.000012	0.731271	8.04	40.4	0.1203	0.511806	0.000011	−16.2	−14.1	2185	2138	−0.4
19MD20a		258	118	6.3493	0.74506	0.000011	0.725631	3.64	16.1	0.1367	0.511826	0.000008	−15.8	−14.2	2606	2143	−0.3
19MD21a		193	180	3.1103	0.734149	0.000009	0.724631	7.67	37.9	0.1223	0.511881	0.000009	−14.8	−12.7	2109	2024	−0.4
19MD26		354	407	2.5209	0.725449	0.000007	0.717735	13.9	73.0	0.1151	0.511988	0.000007	−12.7	−10.4	1792	1839	−0.4
19MD27		330	358	2.6718	0.726055	0.000011	0.717879	12.9	69.9	0.1116	0.511986	0.000010	−12.7	−10.4	1733	1835	−0.4
19MY16		186	114	4.7378	0.744637	0.000009	0.730140	6.85	34.0	0.1218	0.511822	0.000014	−15.9	−13.9	2193	2115	−0.4
19MY17		218	148	4.2768	0.743592	0.000008	0.730505	5.99	28.8	0.1257	0.511888	0.000010	−14.6	−12.7	2178	2021	−0.4
19MY18		211	163	3.7573	0.740284	0.000010	0.728787	6.66	30.3	0.1329	0.511861	0.000011	−15.2	−13.4	2418	2078	−0.3
19MY19		218	137	4.6198	0.742811	0.000007	0.728675	5.99	29.0	0.1249	0.511900	0.000010	−14.4	−12.4	2136	1999	−0.4
19MY20		203	165	3.5710	0.740195	0.000011	0.729267	6.59	31.2	0.1277	0.511864	0.000009	−15.1	−13.2	2269	2063	−0.4
19MY21		166	255	1.8872	0.727566	0.000009	0.721792	10.0	54.1	0.1117	0.511919	0.000013	−14.0	−11.7	1834	1940	−0.4
19MY34	Tachileik	148	64.6	6.6516	0.742951	0.000008	0.719272	6.72	34.3	0.1184	0.511902	0.000011	−14.4	−11.9	1990	1983	−0.4
19MY35		105	131	2.3244	0.730987	0.000009	0.722712	4.92	23.2	0.1282	0.511920	0.000014	−14.0	−11.8	2184	1980	−0.3
19MY36		144	123	3.3962	0.734371	0.000009	0.722281	3.23	14.4	0.1356	0.511909	0.000011	−14.2	−12.3	2411	2016	−0.3
19MY37		132	95.9	3.9933	0.735270	0.000010	0.721054	3.63	16.6	0.1322	0.511897	0.000007	−14.4	−12.4	2331	2025	−0.3
19MY49		136	134	2.9417	0.725808	0.000007	0.715336	6.03	28.6	0.1274	0.511946	0.000012	−13.5	−11.3	2120	1937	−0.4
PM07-7-b1	Yunnan	180	56.6	9.257	0.769752	0.000011	0.736797	6.47	35.7	0.1095	0.511665	0.000008	−19.0	−16.2	2164	2333	−0.4

Note: $\varepsilon_{Nd}(t) = 10{,}000 \times \{[(^{143}Nd/^{144}Nd)_S - (^{147}Sm/^{144}Nd)_S \times (e^{\lambda t}-1)]/[(^{143}Nd/^{144}Nd)_{CHUR,0} - (^{147}Sm/^{144}Nd)_{CHUR} \times (e^{\lambda t}-1)] - 1\}$.
$T_{DM} = 1/\lambda \times \ln\{1 + [(^{143}Nd/^{144}Nd)_S - (^{143}Nd/^{144}Nd)_{DM}]/[(^{147}Sm/^{144}Nd)_S - (^{147}Sm/^{144}Nd)_{DM}]\}$.
$T_{DM2} = T_{DM} - (T_{DM} - t) \times (f_{CC} - f_S)/(f_{CC} - f_{DM})$. $f_S = (^{147}Sm/^{144}Nd)_S/(^{147}Sm/^{144}Nd)_{CHUR} - 1$.
$f_{CC} = (^{147}Sm/^{144}Nd)_{crust}/(^{147}Sm/^{144}Nd)_{CHUR} - 1$. $f_{DM} = (^{147}Sm/^{144}Nd)_{DM}/(^{147}Sm/^{144}Nd)_{CHUR} - 1$.
$(^{147}Sm/^{144}Nd)_{CHUR} = 0.1967$, $(^{143}Nd/^{144}Nd)_{CHUR,0} = 0.512638$.
$(^{147}Sm/^{144}Nd)_{DM} = 0.2137$, $(^{143}Nd/^{144}Nd)_{DM} = 0.51315$, $(^{147}Sm/^{144}Nd)_{crust} = 0.118$.
$(^{87}Sr/^{86}Sr)_i = {^{87}Sr}/{^{86}Sr} - (^{87}Rb/^{86}Sr) \times (e^{\lambda t} - 1)$
$\lambda_{Sm\text{-}Nd} = 0.00654\ Ga^{-1}$. $\lambda_{Rb\text{-}Sr} = 0.0142\ Ga^{-1}$. $t = 215$ Ma for Kyaing Tong granites. $t = 250$ Ma for Tachileik granites. s = sample.
The formulas and parameters were based on literature of Wu et al. (2000)
^{87}Rb/^{86}Sr and ^{147}Sm/^{144}Nd ratios were calculated using Rb, Sr, Sm and Nd contents analyzed by ICP-MS.

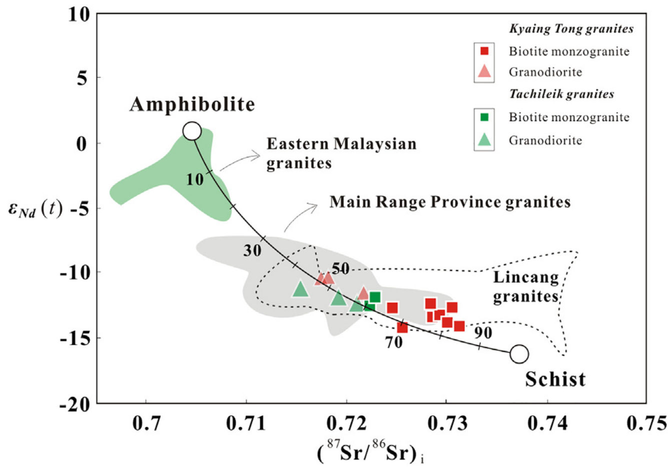

Fig. 8. ε_{Nd} (t) vs $^{87}Sr/^{86}Sr$ isotopic ratio plot of the Kyaing Tong and Tachileik granites showing mixing proportions between two end-members of "Amphibolite" and "Schist". The parameters used are: $\varepsilon_{Nd} = +1.3$, $^{87}Sr/^{86}Sr = 0.705$ for the "Amphibolite" (after *Peng* et al., 2020), and $\varepsilon_{Nd} = -16.2$, $^{87}Sr/^{86}Sr = 0.737$ for the "Schist" of this study (Table 4). Data sources: (1) Eastern Malaysian granites: *Ng* et al., 2015a; (2) Main Range Province granites: *Ng* et al., 2015a; *Wang* et al., 2016; (3) Lincang granites: *Deng* et al., 2018; *Cong* et al., 2020.

environment should show distinctive negative anomalies in Ba, Nb, Ta, Sr, and Ti, as observed in the Kyaing Tong and Tachileik granites (Fig. 7B). Furthermore, U, Th, and K are incompatible in the residual phases produced during dehydration melting reactions (*Rapp and Watson*, 1995; *Sisson* et al., 2005), and the Lancang Group amphibolites show strongly negative Th and U anomalies (Fig. 7D), while the granites show positive anomalies in these elements (Fig. 7D), indicating that amphibolites are a complementary residuum to the granites. In addition, chondrite-normalized REE patterns of the Kyaing Tong and Tachileik granites invariably show light REE fractionation (Fig. 7A), which is consistent with plagioclase being a residual phase. Heavy REE fractionation is not present in any of the rocks studied (Fig. 7A), suggesting that garnet was not an important residual phase in any case. In addition, the REE and trace element patterns in the Kyaing Tong and Tachileik granites resemble those of schist from the Lancang Group (Fig. 7C). This is another important clue for the idea of for wall-rock (schist) assimilation. Furthermore, the Kyaing Tong granites contain abundant xenoliths of two-mica quartz schists (Fig. 3C and D), supporting for this interpretation. Geochemically, most of the Kyaing Tong and Tachileik granites are peraluminous (Fig. 6A), with A/CNK > 1.1, and show S-type characteristics (*Chappell* et al., 2012). We consider that contamination of sedimentary country rocks could explain the S-type characteristics of these granites.

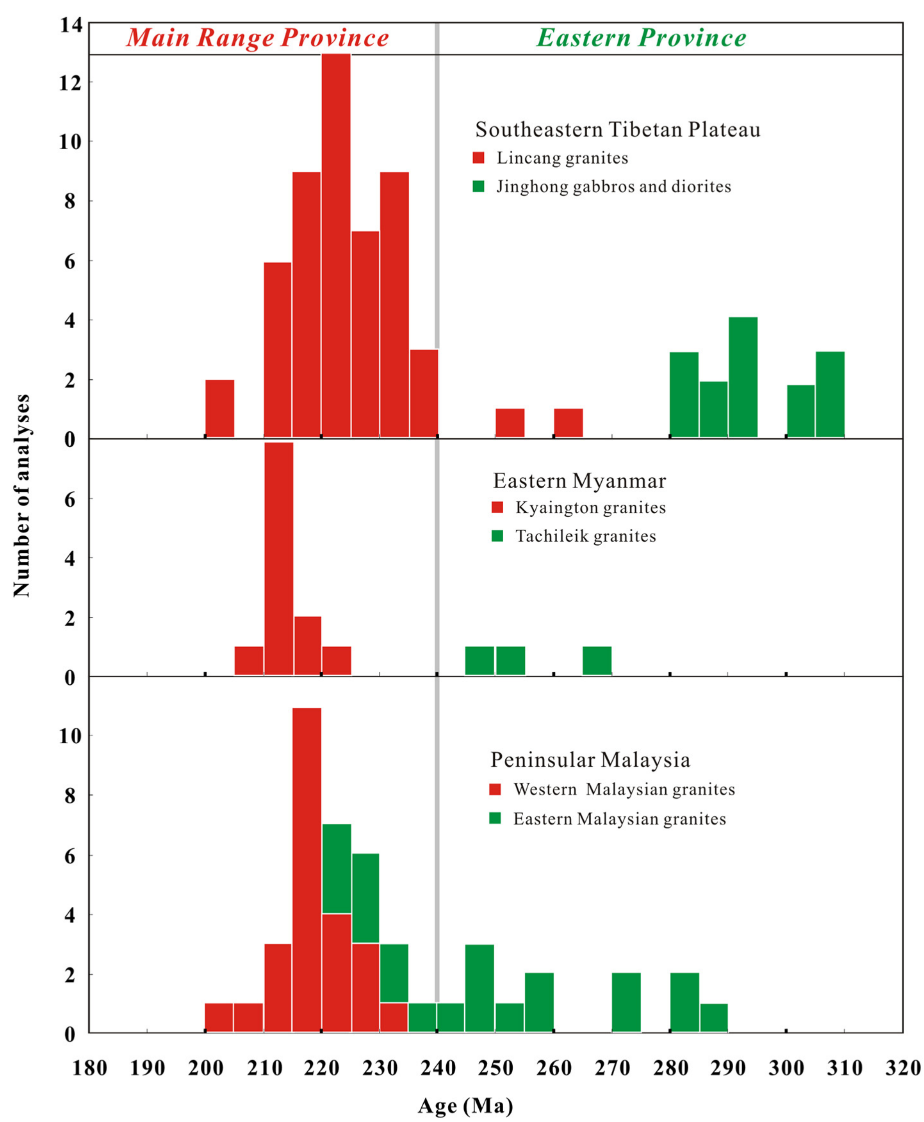

Fig. 9. Comparison of emplacement ages of Main Range and Eastern Province granites in the southeastern Tibetan Plateau, eastern Myanmar, and Peninsular Malaysia. Note that ages of the Main Range Province granites are dominantly from Middle to Late Triassic, spanning 200–240 Ma, whilst Eastern Province granitoids exhibit largely older U–Pb ages ranging from 220 to 290 Ma. Zircon U–Pb data are after Table 5.

Table 5
Summary of age-data of the Main Range and Eastern Province granites in southeastern Tibetan Plateau, eastern Myanmar and Malaysian.

Location	Province	Lithology	Zircon U-Pb	Age (Ma)	References
Southeastern Tibetan Plateau	Main Range	Granite	LA-ICP-MS	228 ± 2 Ma	Wang et al. (2015)
		Granite	LA-ICP-MS	222 ± 1 Ma	
		Granite	LA-ICP-MS	217 ± 2 Ma	Wang et al. (2014)
		Granite	LA-ICP-MS	224 ± 1 Ma	
		Granite	LA-ICP-MS	224 ± 1 Ma	
		Granite	LA-ICP-MS	233 ± 2 Ma	
		Granite	LA-ICP-MS	226 ± 1 Ma	
		Granite	LA-ICP-MS	224 ± 2 Ma	
		Granite	LA-ICP-MS	226 ± 2 Ma	
		Granite	LA-ICP-MS	232 ± 1 Ma	Peng et al. (2013)
		Granite	LA-ICP-MS	233 ± 3 Ma	
		Granite	LA-ICP-MS	232 ± 2 Ma	
		Granite	LA-ICP-MS	234 ± 1 Ma	
		Granite	LA-ICP-MS	229 ± 3 Ma	
		Granite	LA-ICP-MS	239 ± 1 Ma	Hennig et al. (2009)
		Granite	SHRIMP	229 ± 3 Ma	Peng et al. (2006)
		Granite	SHRIMP	230 ± 4 Ma	
		Granite	LA-ICP-MS	219 ± 1 Ma	Kong et al. (2012)
		Granite	LA-ICP-MS	220 ± 1 Ma	
		Granite	LA-ICP-MS	214 ± 2 Ma	Dong et al. (2013)
		Granite	LA-ICP-MS	212 ± 2 Ma	
		Granite	LA-ICP-MS	203 ± 1 Ma	
		Granite	LA-ICP-MS	227 ± 1 Ma	
		Granite	LA-ICP-MS	232 ± 4 Ma	Nie et al. (2012)
		Granite	LA-ICP-MS	216 ± 0.4 Ma	Zhao et al. (2018)
		Granite	LA-ICP-MS	231 ± 1 Ma	Zeng et al. (2018))
		Diorite	LA-ICP-MS	229 ± 1 Ma	
		Granite	LA-ICP-MS	217 ± 3 Ma	Liu et al. (2015)
		Granite	LA-ICP-MS	220 ± 5 Ma	
		Granite	LA-ICP-MS	223 ± 2 Ma	
		Granite	LA-ICP-MS	215 ± 3 Ma	
		Granite	LA-ICP-MS	223 ± 2 Ma	
		Granite	LA-ICP-MS	224 ± 2 Ma	
		Granite	LA-ICP-MS	216 ± 2 Ma	
		Granite	LA-ICP-MS	223 ± 1 Ma	Catlos et al. (2017)
		Granite	LA-ICP-MS	223 ± 1 Ma	
		Granite	LA-ICP-MS	221 ± 0.1 Ma	
		Granite	LA-ICP-MS	218 ± 0.2 Ma	
		Granite	LA-ICP-MS	214 ± 1 Ma	
		Granite	LA-ICP-MS	212 ± 1 Ma	
		Granite	LA-ICP-MS	216 ± 1 Ma	
		Granite	LA-ICP-MS	211 ± 1 Ma	
		Granite	LA-ICP-MS	221 ± 1 Ma	Cong et al., 2020
		Granite	LA-ICP-MS	231 ± 2 Ma	
		Granite	LA-ICP-MS	237 ± 2 Ma	
		Granite	LA-ICP-MS	237 ± 1 Ma	
		Granite	LA-ICP-MS	217 ± 3 Ma	
		Granite	LA-ICP-MS	203 ± 1 Ma	Deng et al. (2018)
	Eastern	Diorite	LA-ICP-MS	300 ± 2.6 Ma	Xu et al. (2016)
		Diorite	LA-ICP-MS	305.7 ± 3.7 Ma	
		Tonalite	SHRIMP	285.8 ± 2 Ma	Jian et al. (2009)
		Gabbro	SHRIMP	285.6 ± 1.7 Ma	
		Anorthosite	LA-ICP-MS	290 ± 2 Ma	Wang et al. (2015)
		Diorite	TIMS	294.9 ± 2.6 Ma	Li et al. (2012)
		Gabbro	LA-ICP-MS	302.6 ± 2 Ma	Zhang et al. (2013)
		Diorite	LA-ICP-MS	321 ± 14 Ma	Sun et al. (2015)
		Diorite	LA-ICP-MS	305.7 ± 9.3 Ma	
		Diorite	LA-ICP-MS	291.3 ± 7.6 Ma	
		Diorite	LA-ICP-MS	307.4 ± 7.3 Ma	
		Granodiorite	LA-ICP-MS	283.7 ± 1.1 Ma	Hennig et al. (2009)
		Granodiorite	LA-ICP-MS	283 ± 1.3 Ma	
		Granodiorite	LA-ICP-MS	282 ± 1.2 Ma	
		Gabbro	LA-ICP-MS	292 ± 1 Ma	
		Granodiorite	LA-ICP-MS	261 ± 1 Ma	Deng et al. (2018)
		Granodiorite	LA-ICP-MS	252 ± 1 Ma	
Eastern Myanmar	Main Range	Granite	LA-ICP-MS	219.3 ± 1.3 Ma	Gardiner et al. (2016)
		Granite	LA-ICP-MS	220.1 ± 1.1 Ma	
		Granite	LA-ICP-MS	214 ± 1.4 Ma	this study
		Granite	LA-ICP-MS	213.6 ± 1.3 Ma	
		Granodiorite	LA-ICP-MS	213.4 ± 1.3 Ma	
		Granodiorite	LA-ICP-MS	212 ± 1.7 Ma	
		Granite	LA-ICP-MS	211.6 ± 1.6 Ma	
		Granite	LA-ICP-MS	215.9 ± 1.2 Ma	
		Granite	LA-ICP-MS	212.4 ± 1.1 Ma	

(continued on next page)

Table 5 (*continued*)

Location	Province	Lithology	Zircon U-Pb	Age (Ma)	References
		Granite	LA-ICP-MS	211.3 ± 1.1 Ma	
		Granite	LA-ICP-MS	210.4 ± 1.4 Ma	
		Granodiorite	LA-ICP-MS	206.7 ± 1.1 Ma	
	Eastern	Granite	LA-ICP-MS	265.8 ± 2.1 Ma	Gardiner et al. (2016)
		Granodiorite	LA-ICP-MS	245.6 ± 1.9 Ma	this study
		Granodiorite	LA-ICP-MS	250.2 ± 1.1 Ma	
Western Malaysian	Main Range	Granite	LA-ICP-MS	209.6 ± 6.7 Ma	Searle et al. (2012)
		Granite	LA-ICP-MS	215.2 ± 6.7 Ma	
		Granite	LA-ICP-MS	225.4 ± 1.3 Ma	Ng et al. (2015a)
		Granite	LA-ICP-MS	218.3 ± 2.4 Ma	
		Granite	LA-ICP-MS	212.1 ± 2.4 Ma	
		Granite	LA-ICP-MS	215.3 ± 2.6 Ma	
		Granite	LA-ICP-MS	215.9 ± 1.7 Ma	
		Granite	LA-ICP-MS	222.4 ± 1.8 Ma	
		Granite	LA-ICP-MS	231.9 ± 0.9 Ma	
		Granite	LA-ICP-MS	220.1 ± 2.8 Ma	Ng et al. (2015b)
		Granite	LA-ICP-MS	219.4 ± 1.5 Ma	
		Granite	LA-ICP-MS	225.4 ± 1.3 Ma	
		Granite	LA-ICP-MS	218.3 ± 2.4 Ma	
		Granite	LA-ICP-MS	220.1 ± 1 Ma	
		Granite	LA-ICP-MS	215.7 ± 1.6 Ma	
		Granite	LA-ICP-MS	213.9 ± 2.9 Ma	
		Granite	LA-ICP-MS	215.5 ± 1.5 Ma	
		Granite	LA-ICP-MS	212.1 ± 2.4 Ma	
		Granite	LA-ICP-MS	215.3 ± 2.6 Ma	
		Granite	LA-ICP-MS	215.9 ± 1.7 Ma	
		Granite	LA-ICP-MS	200.8 ± 2 Ma	
		Granite	LA-ICP-MS	222.4 ± 1.8 Ma	
		Granite	LA-ICP-MS	217.4 ± 1.2 Ma	
		Granite	LA-ICP-MS	226.2 ± 1.2 Ma	
Eastern Malaysian	Eastern	Granite	LA-ICP-MS	257.6 ± 1.6 Ma	Ng et al. (2015a)
		Granite	LA-ICP-MS	284.2 ± 1.6 Ma	
		Granite	LA-ICP-MS	248.4 ± 1.8 Ma	
		Granite	LA-ICP-MS	270 ± 1.4 Ma	
		Granite	LA-ICP-MS	257.6 ± 1.6 Ma	Ng et al. (2015b)
		Granite	LA-ICP-MS	284.2 ± 1.6 Ma	
		Granite	LA-ICP-MS	289.3 ± 2.4 Ma	
		Granite	LA-ICP-MS	247.8 ± 1.7 Ma	
		Granite	LA-ICP-MS	248.4 ± 1.8 Ma	
		Granite	LA-ICP-MS	250.5 ± 1.7 Ma	
		Granite	LA-ICP-MS	270 ± 1.4 Ma	
		Granite	LA-ICP-MS	231 ± 2.6 Ma	
		Granite	LA-ICP-MS	238.5 ± 1.7 Ma	
		Granite	LA-ICP-MS	244.5 ± 3.1 Ma	
		Granite	LA-ICP-MS	222.4 ± 1.8 Ma	
		Granite	LA-ICP-MS	231.8 ± 1.7 Ma	
		Granite	LA-ICP-MS	220.4 ± 3.9 Ma	
		Granite	LA-ICP-MS	222.2 ± 1.8 Ma	
		Granite	LA-ICP-MS	227.2 ± 1.9 Ma	
		Granite	LA-ICP-MS	225.5 ± 2.5 Ma	
		Granite	LA-ICP-MS	226.7 ± 2.2 Ma	

5.3. Extension of the Main Range and Eastern Province granite belts

Within Peninsular Malaysia, the tectonic division between the Main Range and Eastern Province is the Paleo-Tethys Bentong-Raub suture (*Hutchison,* 1975). *Searle* et al. (2012) reported zircon U–Pb ages of 215 ± 7 Ma and 210 ± 7 Ma on Kuala Lumpur granites from the Main Range Province, which places constraints on magmatism related to continental collision and crustal thickening during the Indosinian orogeny. *Ng* et al. (2015a, 2015b) undertook extensive zircon U–Pb geochronology on granitoids from across Peninsular Malaysia. The Eastern Province granitoids in Peninsular Malaysia consist mainly of I-type subduction-related granodiorites, granites, and tonalites, which formed at 220–289 Ma, while Main Range Province granites formed at 201–232 Ma. The Main Range Province of western Malaysia continues north into Thailand, where it occurs dominantly as biotite- and K-feldspar-bearing megacrystic granites of Triassic age that intrude into Ordovician to Devonian sedimentary rocks. In NW Thailand, the granites exhibit an age range of 200–237 Ma (*Gardiner* et al., 2016; *Wang* et al., 2016), which is similar to the age of the Main Range Province granites. The Chiang Rai pluton in NW Thailand is the northernmost of these bodies and extends across the border into Myanmar (*Cobbing* et al., 1986).

The Eastern Province of Malaysia continues northwards to the large batholith of Tak in Thailand (*Cobbing* et al., 1986). The composition of the Tak batholith changes from granodioritic, through monzogranitic to syenogranitic (*Mahawat* et al., 1990). The Chiang Rai Line represents the delineation between the Chiang Rai pluton of Main Range Province and the Tak batholith of Eastern Province in Thailand (*Mitchell,* 1977; *Cobbing* et al., 1986; *Barr and MacDonald,* 1991; *Charusiri* et al., 1993). *Gardiner* et al. (2016) suggested that the Chiang Rai Line extends north into eastern Myanmar. We believe that the Chiang Rai Line has been cut and offset along the Golden Triangle strike-slip fault and becomes less well defined (Fig. 2B). The 207–216 Ma span of our 10 new U–Pb zircon ages from the Kyaing Tong pluton are consistent with the 200–240 Ma age range typical of the Main Range Province (Fig. 9; Table 5). We therefore conclude that the Kyaing Tong granites are part of—and lie within—the northern extension of the Main Range Province, such that these ages provide a firm constraint on the extension of this belt.

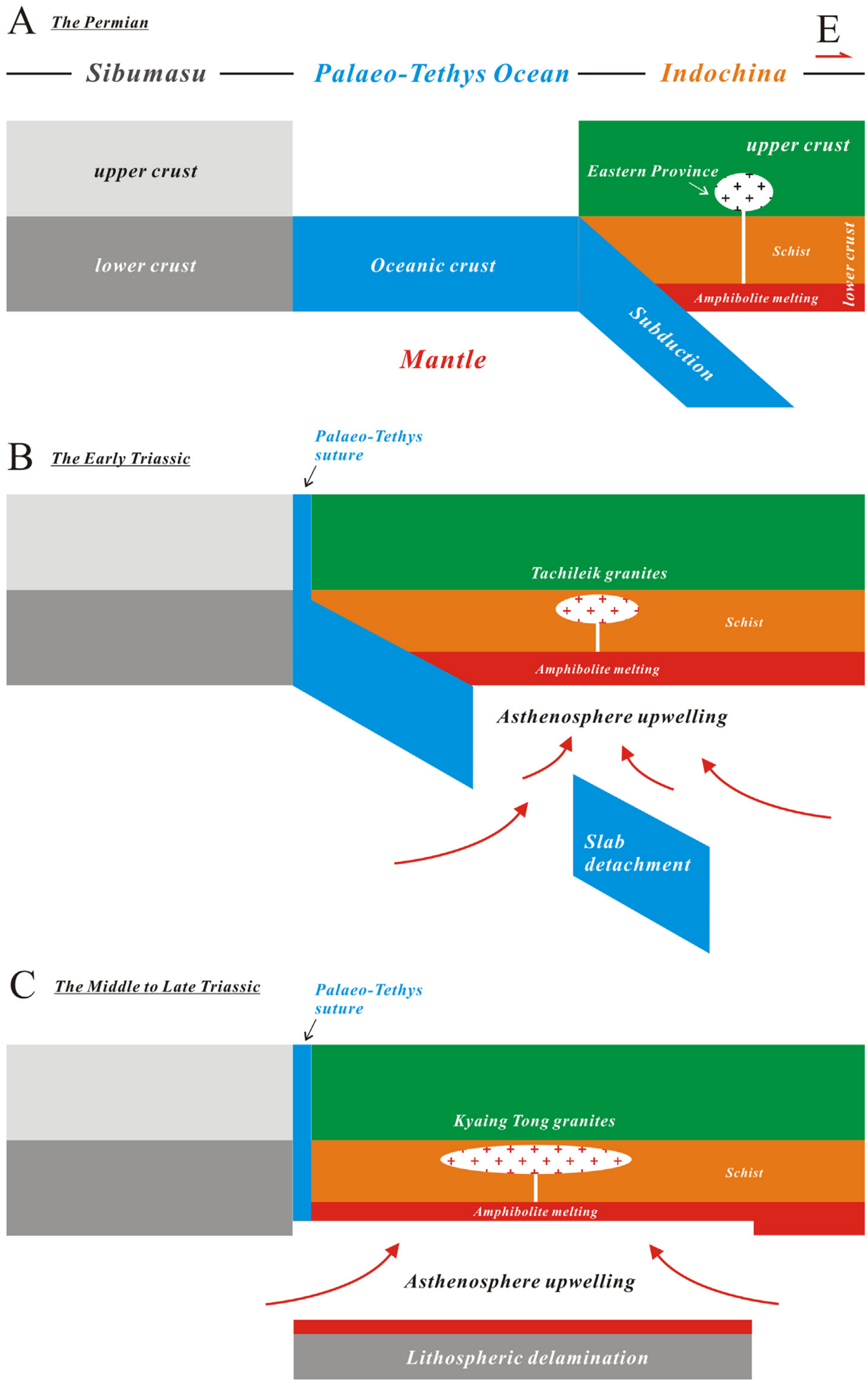

Fig. 10. (A) Tectonic setting for the magma generation of the Main Range and Eastern Province granites in the mainland Southeast Asia.

The Main Range Province continues north into the Lincang batholith in the southeastern Tibetan Plateau. Previous studies on the Lincang granitoids have yielded zircon U–Pb ages ranging from 203 Ma to 235 Ma (Fig. 9; Table 5) (*Cong* et al., 2020; *Dong* et al., 2013; *Hennig* et al., 2009; *Jian* et al., 2009; *Kong* et al., 2012; *Nie* et al., 2012; *Peng* et al., 2006; *Peng* et al., 2013; *Wang* et al., 2014), which exhibit a similar age range to the Main Range Province granites in Peninsular Malaysia and northwest Thailand. Our U–Pb zircon ages from the Tachileik pluton (246–250 Ma) are entirely consistent with the 220–290 Ma age range documented for the Eastern Province (Fig. 9). The Lancangjiang zone in the southeastern Tibetan Plateau lies north of the Tachileik pluton, and is bounded to the east by the Lanping-Simao basin and to the west by the Lincang granites, respectively (*Zhong*, 1998). The Lancangjiang zone is reported to contain granodiorites and diorites emplaced at 282–321 Ma in Jinghong (*Hennig* et al., 2009; *Sun* et al., 2015), diorites and gabbros emplaced at 292–306 Ma in Nanlianshan (*Hennig* et al., 2009; *Xu* et al., 2016), and diorites and gabbros emplaced at 286–303 Ma in Banpo (Fig. 9; Table 5) (*Jian* et al., 2009; *Li* et al., 2012; *Zhang* et al., 2013). These Late Carboniferous–Permian ages match those found further south in the Eastern Province in eastern Myanmar, Peninsular Malaysia, and Singapore (Ng et al., 2015b; Oliver et al., 2011; Searle et al., 2012). Therefore, we consider that the Lancangjiang belt is a possible northern extension of the Eastern Province (Fig. 2B).

5.4. Magmatic evolution of the Main Range and Eastern Province

We consider that the Sibumasu and Indochina terranes collided to close the Paleo-Tethys Ocean during the Early Triassic, according to the following evidence: (1) The Early Triassic deposition is commonly absent, while the pre-Triassic strata are unconformably overlain by the Middle Triassic strata in the Changning-Menglian Paleo-Tethys orogenic belt (Zhong, 1998). (2) Records of Early Triassic ultra-high-pressure metamorphism of blueschists and eclogites have been recognized in the Lancang Group from the southeastern Tibetan Plateau (Fan et al., 2015; Wang et al., 2018). (3) The Middle Triassic Manghuai A-type rhyolites were investigated in the Changning-Menglian Paleo-Tethys orogenic belt (Peng et al., 2013). (4) The Middle–Late Triassic granites occur on both sides of the Bentong-Raub suture (Ng et al., 2015b) and the Changning-Menglian suture (Cong et al., 2020; Nie et al., 2012). (5) The change in geochemistry of volcanic rocks from intermediate in the Permian to felsic in the Middle–Late Triassic in East Malaysia (Metcalfe, 2013b). (6) Slightly deformed Triassic deposits overlaying intensely deformed Paleozoic rocks, and missing latest Permian to earliest Triassic fossils (representing an unconformity) within Permian–Triassic limestones in Sumatra (Barber and Crow, 2009). In this scenario, *syn*-collisional and post-collisional setting is the most feasible mechanism for the generation of the Tachileik and Kyaing Tong granites in eastern Myanmar, respectively. Combining the results of previous studies (Cong et al., 2020; Deng et al., 2018; Dong et al., 2013; Gardiner et al., 2016; Hennig et al., 2009; Heppe et al., 2007; Jian et al., 2009; Liu et al., 2020; Ng et al., 2015a; Peng et al., 2013; Qian et al., 2017; Searle et al., 2012; Wang et al., 2014; Wang et al., 2016; Zhong, 1998), our new zircon U–Pb and Sr–Nd isotopic data support the following model for the magmatic evolution of the Main Range and Eastern Province, which is typically episodic and shows three stages during the Permian to Late Triassic. Firstly, during Paleo-Tethys subduction beneath the Indochina block in the Permian, fluids driven off the subducting slab induced melting of amphibolite of the Indochina block. Buoyant silicic magmas ascended from their deep source regions into the upper crust and crystallized to form the Eastern Province granites (Fig. 10A). These granites included the arc magmatism in the Lancangjiang zone (Hennig et al., 2009; Jian et al., 2009; Li et al., 2012; Sun et al., 2015; Xu et al., 2016; Zhang et al., 2013) and East Malaysia (Ng et al., 2015b; Searle et al., 2012). Further evidence for Paleo-Tethys eastward subduction is provided by the spatial distribution of the Xiaoheijiang low-pressure and Lancang high-pressure metamorphic belts to the east of the Changning-Menglian suture (Zhang et al., 1993; Zhong, 1998). Secondly, the Sibumasu and Indochina blocks collided with each other in the Early Triassic. The collision resulted in the final closure of the Paleo-Tethys Ocean, which is recorded by the Changning-Menglian-Inthanon-Bentong-Raub sutures in the mainland Southeast Asia (Gardiner et al., 2016; Metcalfe, 2000; Sone and Metcalfe, 2008). Slab detchment occurred due to the density increase of the eclogitic slab. Mafic magma formed by upwelling of the asthenosphere would rise into the lower crust of the Indochina block, where it further induced crustal melting. This study suggests that the Tachileik pluton was derived from partial melting of the amphibolite and underwent wall-rock assimilation of two-mica quartz schist in the Early Triassic (Fig. 10B). Meanwhile, rapid exhumation of high-pressure rocks would be induced by slab detchment within the Changning-Menglian Paleo-Tethys orogenic belt (Zhong, 1998). Finally, the lower crust of the Sibumasu block was subducted beneath the Indochina block. Lithospheric delamination of Paleo-Tethys orogen occurred in the Middle to Late Triassic because the high density of thickened lower crust led to it becoming gravitationally unstable. Mafic magma formed by upwelling of the asthenosphere would rise into the lower crust of the Indochina block, where it further induced large-scale crustal melting and formation of the Main Range Province granites (Fig. 10C). Their Sr–Nd isotope values suggest that the Kyaing Tong granites were derived from partial melting of the amphibolite and underwent assimilation of two-mica quartz schist of Lancang Group. Development of the Late Triassic–Early Jurassic molasse and continental red-bed sequence marked the termination of the Indosinian orogeny in the mainland Southeast Asia.

6. Conclusions

We present new LA-ICP-MS zircon U–Pb ages for 12 granitoids of the Kyaing Tong and Tachileik plutons in eastern Myanmar. The Tachileik granites have an age range of 246–250 Ma and are interpreted to have formed due to collision of Sibumasu with the Indochina continent, which closed Paleo-Tethys Ocean along the Paleo-Tethys suture. Post-collisional Kyaing Tong granites intruded along the Paleo-Tethys orogenic belt over a restricted period during the Late Triassic (207–216 Ma). We consider that both the Kyaing Tong and Tachileik granites are of I-type affinity. Their Sr–Nd isotope values suggest that the Tachileik and Kyaing Tong plutons were derived from partial melting of the amphibolite and underwent assimilation of two-mica quartz schist.

Declaration of Competing Interest

None.

Acknowledgements

This study was supported by the National Nature Science Foundation of China (project No. 41888101), Science and Technology Foundation of Guizhou Province (project No. [2011]2360), and China Geological Survey (project No. DD20190053). Yue-Heng Yang, Ping Xiao and Lei Xu are gratefully thanked for instrument analyses.

References

MGS (Myanmar Geosciences Society), 2014. 1:2,250,000 Geological map of Myanmar.

Barber, A.J., Crow, M.J., 2009. Structure of Sumatra and its implications for the tectonic assembly of Southeast Asia and the destruction of Paleotethys. Island Arc 18, 3–20.

Barr, S.M., MacDonald, A.S., 1991. Toward a late Palaeozoic-early Mesozoic tectonic model for Thailand. Thailand Journal of Geosciences 1, 11–22.

Boehnke, P., Watson, E.B., Trail, D., Harrison, T.M., Schmitt, A.K., 2013. Zircon saturation re-revisited. Chem. Geol. 351, 324–334.

Carter, A., Roques, D., Bristow, C., Kinny, P., 2001. Understanding Mesozoic accretion in Southeast Asia: significance of Triassic thermotectonism (Indosinian orogeny) in Vietnam. Geology 29 (3), 211–214.

Catlos, E.J., Reyes, E., Brookfield, M., Stockli, D.F., 2017. Age and emplacement of the Permian-Jurassic Menghai batholith, Western Yunnan, China. International Geology Review 59 (8), 919–945.

Chappell, B.W., White, A.J.R., 1974. Two contrasting granite types. Pacific Geology 8, 173–174.

Chappell, B.W., Bryant, C.J., Wyborn, D., 2012. Peraluminous I-type granites. Lithos 153, 142–153.

Charusiri, P., Clark, A.H., Farrar, E., Archibald, D., Charusiri, B., 1993. Granite belts in Thailand: evidence from the $^{40}Ar/^{39}Ar$ geochronological and geological syntheses. Journal of Southeast Asian Earth Sciences 8 (14), 127–136.

Chen, F., Li, X.H., Wang, X.L., Li, Q.L., Siebel, W., 2007. Zircon age and Nd-Hf isotopic composition of the Yunnan Tethyan belt, southwestern China. International Journal of Earth Sciences 96, 1179–1194.

Cobbing, E.J., Mallick, D.I.J., Pitfield, P.E.J., Teoh, L.H., 1986. The granites of the Southeast Asia Tin Belt. Journal of the Geological Society, London 143, 537–550.

Cong, F., Wu, F.Y., Li, W.C., Mou, C.L., Huang, X.M., Wang, B.D., Hu, F.Y., Peng, Z.M., 2020. Origin of the Triassic Lincang Granites in the Southeastern Tibetan Plateau: Crystallization from crystal mush. Lithos https://doi.org/10.1016/j.lithos.2020.105452.

Deng, J., Wang, C.M., Zi, J.W., Xia, R., Li, Q., 2018. Constraining subduction-collision processes of the Paleo-Tethys along the Changning-Menglian Suture: New zircon U-Pb ages and Sr-Nd-Pb-Hf-O isotopes of the Lincang Batholith. Gondw. Res. 62, 75–92.

Dong, G.C., Mo, X.X., Zhao, Z.D., Zhu, D.C., Goodman, R.C., Kong, H.L., Wang, S., 2013. Zircon U-Pb dating and the petrological and geochemical constraints on Lincang granite in Western Yunnan, China: Implications for the closure of the Paleo-Tethys Ocean. J. Asian Earth Sci. 62, 282–294.

Dufek, J., Bergantz, G.W., 2005. Lower Crustal Magma Genesis and Preservation: a Stochastic Framework for the Evaluation of Basalt-Crust Interaction. J. Petrol. 46 (11), 2167–2195.

Fan, W.M., Wang, Y.J., Zhang, Y.H., Zhang, Y.Z., Jourdan, F., Zi, J.W., Liu, H.C., 2015. Paleotethyan subduction process revealed from Triassic blueschists in the Lancang tectonic belt of Southwest China. Tectonophysics 662, 95–108.

Gardiner, N.J., Searle, M.P., Robb, L.J., Morley, C.K., 2015. Neo-Tethyan magmatism and metallogeny in Myanmar-an Andean analogue? J. Asian Earth Sci. 106, 197–215.

Gardiner, N.J., Searle, M.P., Morley, C.K., Whitehouse, M.P., Spencer, C.J., Robb, L.J., 2016. The closure of Palaeo-Tethys in Eastern Myanmar and Northern Thailand: New insights from zircon U-Pb and Hf isotope data. Gondw. Res. 39, 401–422.

Gardiner, N.J., Searle, M.P., Morley, C.K., Robb, L.J., Whitehouse, M.J., Roberts, N.M.W., Kirkland, C.L., Spencer, C.J., 2018. The crustal architecture of Myanmar imaged through zircon U-Pb, Lu-Hf and O isotopes: Tectonic and metallogenic implications. Gondw. Res. 62, 27–60.

Ghani, A.A., Searle, M., Robb, L., Chung, S.L., 2013. Transitional I S type characteristic in the Main Range Granite, Peninsular Malaysia. J. Asian Earth Sci. 76, 225–240.

Hennig, D., Lehmann, B., Frei, D., Belyatsky, B., Zhao, X.F., Cabral, A.R., Zeng, P.S., Zhou, M.F., Schmidt, K., 2009. Early Permian seafloor to continental arc magmatism in the eastern Paleo-Tethys: U-Pb age and Nd-Sr isotope data from the southern Lancangjiang zone, Yunnan, China. Lithos 113, 408–422.

Heppe, K., Dietrich, H., Wemmer, K., 2007. The Lancang River Zone of southwestern Yunnan, China: a questionable location for the active continental margin of Paleotethys. J. Asian Earth Sci. 30, 706–720.

Hutchison, C.S., 1975. Ophiolite in Southeast Asia. Geol. Soc. Am. Bull. 86, 797–806.

Hutchison, C.S., 1977. Granite emplacement and tectonic subdivision in Peninsular Malaysia. Bulletin of the Geological Society of Malaysia 9, 187–207.

Jian, P., Liu, D.Y., Kröner, A., Zhang, Q., Wang, Y.Z., Sun, X.M., Zhang, W., 2009. Devonian to Permian plate tectonic cycle of the Paleo-Tethys Orogen in Southwest China (I): Geochemistry of ophiolites, arc/back-arc assemblages and within-plate igneous rocks. Lithos 113, 748–766.

Kong, H.L., Dong, G.C., Mo, X.X., Zhao, Z.D., Zhu, D.C., Wang, S., Li, R., Wang, Q.L., 2012. Petrogenesis of Lincang granites in Sanjiang area of western Yunnan Province: Constraints from geochemistry, zircon U-Pb geochronology and Hf isotope. Acta Petrol. Sin. 28 (5), 1438–1452 (in Chinese).

Lepvrier, C., Maluski, H., Tich, V.V., Leyreloup, A., Thi, P.T., Vuong, N.V., 2004. The early Triassic Indosinian orogeny in Vietnam (Truong Son Belt and Kontum Massif); implications for the geodynamic evolution of Indochina. Tectonophysics 393, 87–118.

Li, G.Z., Su, S.G., Duan, X.D., 2012. Precise ID-TIMS zircon U-Pb age, whole-rock geochemistry and plate tectonic setting of the Banpo complex in the southern Lancangjiang arc terrane, Sanjiang area, SW China. Earth Science Frontiers 19 (4), 96–109 (in Chinese).

Liu, Y.S., Hu, Z.C., Gao, S., Günther, D., Xu, J., Gao, C.G., Chen, H.H., 2008. In situ analysis of major and trace elements of anhydrous minerals by LA-ICP-MS without applying an internal standard. Chem. Geol. 257, 34–43.

Liu, D.L., Huang, Q.S., Shi, R.D., Yue, Y.H., Ding, L., 2015. Zircon germanium and age constrains on source of Lincang germanium deposit, Yunnan Province. Mineral Deposits 34 (1), 139–148 (in Chinese).

Liu, L., Hu, R.Z., Zhong, H., Yang, J.H., Kang, L.F., Zhang, X.C., Fu, Y.Z., Mao, W., Tang, Y.W., 2020. Petrogenesis of multistage S-type granites from the Malay Peninsula in the Southeast Asian tin belt and their relationship to Tethyan evolution. Gondw. Res. 84, 20–37.

Macdonald, A.S., Barr, S.M., Dunning, G.R., Yaowanoiyothin, W., 1993. The Doi Inthanon metamorphic core complex in NW Thailand: age and tectonic significance. Journal of Southeast Asian Earth Sciences 8 (1–4), 117–125.

Mahawat, C., Atherton, M.P., Brotherton, M.S., 1990. The Tak Batholith, Thailand: the evolution of contrasting granite types and implications for tectonic setting. Journal of Southeast Asian Earth Sciences 4 (1), 11–27.

Metcalfe, I., 2000. The Bentong-Raub suture zone. J. Asian Earth Sci. 18, 691–712.

Metcalfe, I., 2011. Tectonic framework and Phanerozoic evolution of Sundaland. Gondw. Res. 19, 3–21.

Metcalfe, I., 2013a. Gondwana dispersion and Asian accretion: Tectonic and palaeogeographic evolution of eastern Tethys. J. Asian Earth Sci. 66, 1–33.

Metcalfe, I., 2013b. Tectonic evolution of the Malay Peninsula. J. Asian Earth Sci. 76, 195–213.

Mitchell, A.H.G., 1977. Tectonic settings for the emplacement of the Southeast Asian tin granites. Geological Society of Malaysia Bulletin 9, 123–140.

Mitchell, A.G.H., Htay, M.T., Htun, K.M., Win, M.N., Oo, T., Hliang, T., 2007. Rock relationships in the Mogok metamorphic belt, Tatkon to Mandalay, Central Myanmar. J. Asian Earth Sci. 29, 891–910.

Morley, C.K., 2012. Late Cretaceous-early Palaeogene tectonic development of SE Asia. Earth-Science Reviews 115, 37–75.

Mortazavi, M., Sparks, R.S.J., 2004. Origin of rhyolite and rhyodacite lavas and associated mafic inclusions of Cape Akrotiri, Santorini: the role of wet basalt in generating calcalkaline silicic magmas. Contrib. Mineral. Petrol. 146, 397–413.

Ng, S.W.P., Chung, S.L., Robb, L.J., Searle, M.P., Ghani, A.A., Whitehouse, M.J., Oliver, G.J.H., Sone, M., Gardiner, N.J., Roselee, M.H., 2015a. Petrogenesis of Malaysian granitoids in the Southeast Asian tin belt: part 1 Geochemical and Sr-Nd isotopic characteristics. Geological Society of America Bulletin https://doi.org/10.1130/B31213.1.

Ng, S.W.P., Whitehouse, M.J., Searle, M.P., Robb, L.J., Ghani, A.A., Chung, S.L., Oliver, G.J.H., Sone, M., Gardiner, N.J., Roselee, M.H., 2015b. Petrogenesis of Malaysian granitoids in the Southeast Asian tin belt: part 2 U-Pb zircon geochronology and tectonic model. Geological Society of America Bulletin https://doi.org/10.1130/B31214.1.

Nie, F., Dong, G.C., Mo, X.X., Zhu, D.C., Dong, M.L., Wang, X., 2012. Geochemistry, zircon U-Pb chronology of the Triassic granites in the Changning-Menglian suture zone and their implications. Acta Petrol. Sin. 28 (5), 1465–1476 (in Chinese).

Oliver, G.J.H., Khin, Z., Hotson, M.D., 2011. Dating rocks in Singapore: Plate tectonics between 280 and 200 million years ago. Innovation Magazine 10 (2), 2–5.

Patiño, D.A.E., 1999. What do experiments tell us about the relative contributions of crust and mantle to the origin of granitic magmas? Geological Society, London. Special Publications 168 (1), 55–75.

Peng, T.P., Wang, Y.J., Fan, W.M., Liu, D.Y., Shi, Y.R., Miao, L.C., 2006. SHRIMP zircon U-Pb geochronology of early Mesozoic felsic igneous rocks from the southern Lancangjiang and its tectonic implications. Science in China Series D: Earth Sciences 49 (10), 1032–1042.

Peng, T.P., Wilde, S.A., Wang, Y.J., Fan, W.M., Peng, B.X., 2013. Mid-Triassic felsic igneous rocks from the southern Lancangjiang Zone, SW China: Petrogenesis and implications for the evolution of Paleo-Tethys. Lithos 168-169, 15–32.

Peng, Z.M., Fu, Y.Z., Wang, G.Z., Guan, J.L., Geng, Q.R., Hu, J.F., Liu, Y.H., Zhang, Z., 2020. The results of geochronological, geochemical and Sr-Nd-Hf isotopic investigations on amphibolites in the Qingping Region, Changning-Menglian Suture Zone. Acta Geol. Sin. 94 (2), 511–526 (in Chinese).

Pichavant, M., Martel, C., Bourdier, J.-L., Scaillet, B., 2002. Physical conditions, structure, and dynamics of a zoned magma chamber: Mount Pelée (Martinique, Lesser Antilles Arc). J. Geophys. Res. 107 (B5), 2093. https://doi.org/10.1029/2001JB000315.

Qian, X., Feng, Q.L., Wang, Y.J., Zhao, T.Y., Zi, J.W., Udchachon, M., Wang, Y.K., 2017. Late Triassic post-collisional granites related to Paleotethyan evolution in SE Thailand: Geochronological and geochemical constraints. Lithos 286-287, 440–453.

Rapp, R.P., Watson, E.B., 1995. Dehydration Melting of Metabasalt at 8-32 kbar: Implications for Continental Growth and Crust-Mantle Recycling. J. Petrol. 36 (4), 891–931.

Schwartz, M.O., Rajah, S.S., Askury, A.K., Putthapiban, P., Djaswadi, S., 1995. The Southeast Asian Tin Belt. Earth-Science Reviews 38, 95–293.

Searle, M.P., Noble, S.R., Cottle, J.M., Waters, D.J., Mitchell, A.H.G., Hlaing, T., Horstwood, M.S.A., 2007. Tectonic evolution of the Mogok metamorphic belt, Burma (Myanmar) constrained by U-Th-Pb dating of metamorphic and magmatic rocks. Tectonics 26, TC3014. https://doi.org/10.1029/2006TC002083.

Searle, M.P., Whitehouse, M.J., Robb, L.J., Ghani, A.A., Hutchison, C.S., Sone, M., Ng, S.W.P., Roselee, M.H., Chung, S.L., Oliver, G.J.H., 2012. Tectonic evolution of the Sibumasu-Indochina terrane collision zone in Thailand and Malaysia: constraints from new U-Pb zircon chronology of SE Asian tin granitoids. Journal of the Geological Society, London 169, 489–500.

Sisson, T.W., Ratajeski, K., Hankins, W.B., Glazner, A.F., 2005. Voluminous granitic magmas from common basaltic sources. Contrib. Mineral. Petrol. 148, 635–661.

Sone, M., Metcalfe, I., 2008. Parallel Tethyan sutures in mainland Southeast Asia: New insights for Palaeo-Tethys closure and implications for the Indosinian orogeny. C. R. Geosci. 340, 166–179.

Sun, S.S., McDonough, W.F., 1989. Chemical and isotopic systematics of oceanic basalts: implications for mantle composition and processes. In: Saunders, a.D., and Norry, M.J., ed. Magmatism in the ocean basins. Geol. Soc. Lond. Spec. Publ. 42, 313–345.

Sun, Z.B., Lv, X.P., Yu, S.Y., Liu, J.P., Tian, S.M., Li, X.G., 2015. Zircon U-Pb Ages and Petrogeochemical Characteristics of Manxiu Diorite Pluton, Jinghong City, Yunnan Province, China. Acta Mineralogia Sinica 35 (4), 473–480 (in Chinese).

Wang, F., Liu, F.L., Liu, P.H., Shi, J.R., Cai, J., 2014. Petrogenesis of Lincang granites in the south of Lancangjiang area: Constrain from geochemistry and zircon U-Pb geochronology. Acta Petrol. Sin. 30 (10), 3034–3050 (in Chinese).

Wang, C.M., Deng, J., Santosh, M., Lu, Y.J., McCuaig, T.C., Carranza, E.J.M., Wang, Q.F., 2015. Age and origin of the Bulangshan and Mengsong granitoids and their significance for post-collisional tectonics in the Changning-Menglian Paleo-Tethys Orogen. J. Asian Earth Sci. 113, 656–676.

Wang, Y.J., He, H.Y., Cawood, P.A., Srithai, B., Feng, Q.L., Fan, W.M., Zhang, Y.Z., Qian, X., 2016. Geochronological, elemental and Sr-Nd-Hf-O isotopic constraints on the petrogenesis of the Triassic post-collisional granitic rocks in NW Thailand and its Paleotethyan implications. Lithos 266-267, 264–286.

Wang, H.N., Liu, F.L., Li, J., Sun, Z.B., Ji, L., Tian, Z.H., Liu, L.S., Santosh, M., 2018. Petrology, geochemistry and P-T-t path of lawsonite-bearing retrograded eclogites in the Changning-Menglian orogenic belt, southeast Tibetan Plateau. J. Metam. Geol. https://doi.org/10.1111/jmg. 12462.

Watson, E.B., Harrison, T.M., 1983. Zircon saturation revisited: temperature and composition effects in a variety of crustal magma types. Earth Planet. Sci. Lett. 64, 295–304.

Whalen, J.B., Currie, K.L., Chappell, B.W., 1987. A-type granites: geochemical characteristics, discrimination and petrogenesis. Contrib. Mineral. Petrol. 95, 407–419.

Wolf, M.B., Wyllie, P.J., 1994. Dehydration-melting of amphibolite at 10 kbar: the effects of temperature and time. Contrib. Mineral. Petrol. 115, 369–383.

Wu, F.Y., Jahn, B.M., Wilde, S., Sun, D.Y., 2000. Phanerozoic crustal growth: U-Pb and Sr-Nd isotopic evidence from the granites in northeastern China. Tectonophysics 328, 89–113.

Xu, Y.G., Yang, Q.J., Lan, J.B., Luo, Z.Y., Huang, X.L., Shi, Y.R., Xie, L.W., 2012. Temporal-spatial distribution and tectonic implications of the batholiths in the Gaoligong-Tengliang-Yingjiang area, western Yunnan: Constraints from zircon U-Pb ages and Hf isotopes. J. Asian Earth Sci. 53, 151–175.

Xu, G.X., Liu, G.C., Liu, J.P., Tian, S.M., 2016. The U-Pb age and Significancse of zircon in Nanlianshan diorite body in Jinghong, Yunnan. Yunnan Geology 35 (2), 131–136 (in Chinese).

Zeng, W.T., Sun, Z.B., Zhou, K., Wu, J.L., Huang, L., Zhao, J.T., 2018. U-Pb dating of the detrital zircons in the dark dioritic enclaves from the Lincang granites in Mengku, Shuangjiang, western Yunnan and its geological significance. Sedimentary Geology and Tethyan Geology 38 (1), 23–36 (in Chinese).

Zhang, R.Y., Cong, B.L., Maruyamma, S., Liou, J.G., 1993. Metamorphism and tectonic evolution of the Lancang paired metamorphic belts, South-Western China. Journal of the metamorphic Geology 11, 605–619.

Zhang, H., Jin, C.H., Fan, W.Y., Shen, Z.W., Zhang, Y., Cao, J.H., 2013. Zircon LA-ICP-MS U-Pb dating of gabbro of the Banpo Pt-Pd-polymetallic deposit in Jinggu, Yunnan Province, and its geological significance. Geology in China 40 (5), 1433–1442 (in Chinese).

Zhao, F., Li, G.J., Zhang, P.F., Wang, C.B., Sun, Z.B., Tang, X., 2018. Petrogenesis and tectonic implications of the Lincang batholith in the Sanjiang, Southwest China: Constraints by geochemistry, zircon U-Pb chronology and Hf isotope. Acta Petrol. Sin. 34 (5), 1397–1412 (in Chinese).

Zhong, D.L., 1998. The Paleotethys Orogenic Belt in West of Sichuan and Yunnan. Science Publishing House, Beijing, pp. 1–230 (in Chinese).